Geological constraints on the mechanisms of slow earthquakes

James D. Kirkpatrick[1*], Åke Fagereng[2], and David R. Shelly[3]

1. Department of Earth and Planetary Sciences, McGill University, Montreal, H3A 0E8, Canada

2. School of Earth & Ocean Sciences, Cardiff University, Cardiff, CF10 3AT, UK

3. U.S. Geological Survey, 1711 Illinois St, Golden, Colorado, 80401, USA

* corresponding author: james.kirkpatrick@mcgill.ca

The discovery of slow earthquakes over 20 years ago transformed understanding of how plate motions are accommodated at major plate boundaries. Slow earthquakes, which slip more slowly than regular earthquakes but faster than plate motion velocities, occur in a range of tectonic and metamorphic settings. They exhibit spatial and temporal associations with large seismic events that indicate a causal relation between modes of slip at different slip rates. Defining the physical controls on slow earthquakes is therefore critical for understanding fault and shear zone mechanics. In this Review, we synthesize geological observations of a suite of ancient structures that were active in tectonic settings comparable to where slow earthquakes are observed today. The results indicate that a range of grain-scale deformation mechanisms accommodate deformation at low effective stresses in regions generating slow earthquakes. Material heterogeneity and the geometry of structures that form at different inferred strain rates are common to faults and shear zones in multiple tectonic environments, and may represent key attributes that limit slow earthquake slip rates. Further work is needed to resolve how the spectrum of slow earthquake slip rates can arise from different grain-scale deformation mechanisms and whether there is one universal rate-limiting mechanism that defines slow earthquake slip.

[H1] Introduction

Slow earthquakes are a category of slip events with longer durations than 'regular' earthquakes of comparable size[1]. The longest-duration events, referred to as slow slip events (SSEs), last for days to years and do not cause ground shaking (they are aseismic), but the permanent surface offsets they cause are observed geodetically. Shorter-duration events (up to hundreds of seconds) such as low and very low frequency earthquakes (LFEs) and tectonic tremor[2] **[G]**, which is inferred to represent bursts of LFEs[3], are observed seismically. Geodetically and seismologically observed slow earthquakes typically occur in approximately the same fault areas and are sometimes temporally associated[4]. Consequently, seismologically observed slow earthquakes are generally thought to occur when there is an accompanying geodetically observed slow earthquake and they are considered different manifestations of the same deformation process[1,5]. Slow earthquake slip rates encompass a spectrum from ~10^{-7} - ~10^{-6} ms^{-1} for SSEs to ~10^{-3} ms^{-1} for LFEs. They therefore represent transient increases in slip rate above the long-term average level (referred to as plate-rate or continuous aseismic creep, which is typically associated with slip rates of centimeters per year or ~10^{-10} ms^{-1}) and below slip velocities of regular earthquakes (10^{0} ms^{-1}). Whether or not the spectrum of slip rates is continuous from SSE rates to seismic slip rates is still debated[6,7].

Seismological and geodetic data show the signatures of slow earthquakes are similar across settings[1,8], implying slow earthquakes are a fundamental process within many faults. Slow earthquakes are observed near the plate interface in multiple subduction zones and transform margins. They are also located within accretionary wedges **[G]** at subduction zones[9-16] and on a

variety of continental transform[17-22] and extensional faults[23]. In some subduction zones, SSEs accommodate a substantial portion of the plate motion budget[24], indicating that they load or unload the seismogenic zone defined by the nucleation of regular earthquakes[25]. Slow earthquakes have been observed to precede some large magnitude seismic events[26] and are also co-located with regions that accommodate seismic slip[27,28], indicating a causal relation between modes of slip at different slip rates. The recognition of slow earthquakes therefore provides important new constraints on the processes and mechanics of fault slip[24,25,29,30].

Geological observations of ancient, exhumed faults and shear zones that hosted slow earthquakes in the past are uniquely able to provide direct information on the physical mechanisms, fault properties, and deformation conditions that control slow slip[31], which are beyond the resolution of geophysical and geodetic methods. However, there is no clear paleo-speedometer for creep transients and currently no widely accepted, unequivocal evidence for slow earthquakes in the geological record. Furthermore, recent laboratory experiments show that slow earthquakes can arise from a variety of mechanisms, including purely frictional grain boundary sliding[32-34] and viscous deformation accompanied by fracture[35]. Recent studies have proposed potential structures that represent slow slip and highlighted processes or mechanisms relevant to individual settings[36-44], but geological insights into the physical processes and material properties at the slow earthquake source are limited.

In this Review, we synthesize observations of exhumed deformation structures that might be examples of geological records of slow earthquakes from a range of tectonic settings. We aim to establish the physical characteristics of potential slow earthquake sources and compare

geological evidence to the geophysical constraints on the structures that generate slow earthquakes. We focus this work on the environments of seismologically observed slow earthquakes, which we treat as representative of systems that can exhibit the full spectrum of slow earthquake slip rates. Our approach is based on recognizing that slow earthquakes are a general, commonly occurring manifestation of active faulting[8], so ancient exhumed structures must contain a record of their occurrence, even if a specific signature of slow earthquakes has not been recognized. The results emphasize that no single mineral assemblage, deformation structure, or deformation mechanism that controls slow earthquakes. This Review highlights the need for further geologically focused work to identify how the spectrum of slow slip rates can be generated across a diverse range of tectonic settings.

[H1] Geophysical insights into slow earthquake geology

In this section, we review geophysical and seismological data that facilitate predictions regarding the geological characteristics of slow earthquakes[45-47]. The goals are to (1) establish their tectonic contexts to facilitate selection of appropriate ancient exhumed systems for comparison; and (2) predict the geological characteristics of slow earthquake structures to constrain the potential signatures of slow slip in complexly deformed rocks (Table 1).

[H2] Tectonic settings

Seismologically observed slow earthquakes commonly occur on major plate boundaries[3,48-51], though geophysical methods cannot establish whether they originate from a single fault interface or a distributed network of faults or shear zones. Slow earthquakes occur over a very large range of metamorphic conditions (FIG. 1). They are commonly[25,52], but not exclusively[14,53,54], located

in transitional regions at the edges of seismogenic zones[55]. However, globally, hypocentral depths range from ~2 to 45 km and hypocenters also span tens of kilometers along the downdip direction of some individual fault zones[56,57]. Observations of geodetically observed slow earthquakes are less numerous, but inversions of geodetic data show a similar range in depth of slip[27,29,58]. Slow earthquakes therefore occur at all temperatures from near surface to around 700 °C, which implies that different grain-scale deformation mechanisms likely accommodate deformation at the sources of slow earthquakes because the typical constitutive relations for frictional sliding, diffusion creep **[G]**, and crystal-plastic deformation **[G]** are pressure and temperature dependent[59].

Slow earthquakes occur frequently on some well-instrumented plate boundaries, indicating evidence for them should be common in the rock record. For example, around 10^5 slow earthquakes are detected seismically per year each on the San Andreas Fault[60,61] and Nankai[62] and Cascadia[63] subduction zones. Given the areas of the zones hosting slow earthquakes on these faults, 10^5 nucleation sites would, on average, result in millions or tens of millions of slow earthquake events per kilometer cubed per million years. All of these events would result in permanent deformation. However, the number of structures that record these events in an exhumed example will be variable as slow earthquakes are likely hosted on a mixture of new and reactivated structures, and not all structures are preserved in recognizable form. Because seismologically observed slow earthquakes are commonly spatially clustered[49,61,64], some regions within the host deformation zones are expected to contain higher concentrations of related structures. Additionally, deformation that occurred at slow slip rates can be expected to

predominate if structures are exhumed from regions where SSEs account for a significant portion of the total relative plate motions.

[H2] Kinematics and strain rates

Structures recording slow earthquakes must exhibit dominantly shear offset to be consistent with geodetic observations and the double-couple source mechanisms **[G]** of LFEs[3,48,50,65,66]. Slip during a seismologically observed slow earthquake is estimated to be ~0.01–0.1 mm, and the radius of a rupture ranges from ~10 m up to around 200 to 600 m [49,65,67-69]. Inferred stress drops are of the order of 10 – 100 kPa[67], orders of magnitude smaller than the median observed value of approximately 4 MPa for regular earthquakes[70].

The strain rates associated with slow earthquakes depend on the thickness of the slip zone across which the slip is distributed. Assuming simple shear, strain rate can be approximated as the ratio of the slip rate to slip zone thickness. Slip rates of 10^{-3} ms^{-1} therefore imply strain rates of 10^{-5}, 10^{0}, or 10^{3} s^{-1} for representative slip zone thicknesses of 100 m, 1 mm, and 1 µm, respectively. SSE average slip rates of ~10^{-7} ms^{-1}, give strain rates of 10^{-9}, 10^{-4}, or 10^{-1} s^{-1} for thicknesses of 100 m, 1 mm, and 1 µm, respectively. These average rates can, however, also be achieved by multiple, faster slip increments, too small to be distinguished geodetically and spaced out over the duration of a single recorded slip episode[71]. Because slip at rates spanning the spectrum of slow earthquakes are often detected in the same place, the structures resulting from these different strain rates could be mutually crosscutting, or overprinting, unless they are spatially separated and subparallel.

[H2] Deformation conditions

Substantial geophysical evidence indicates that source regions of slow earthquakes experience high pore fluid pressure and low effective stress[46,72,73]. The evidence includes seismic wave velocities that imply low Poisson's ratio[74-76] and the sensitivity of small earthquakes to small perturbations in stress from tidal loading or teleseismic waves[77,78]. Together, these observations indicate that structures hosting slow earthquakes are critically stressed **[G]**[47,79,80]. In some cases, tremor migrates at rates of ~1 – 100 km/hr[81,82], suggesting mechanical connection or similar proximity to failure across source regions up to around 100 km apart[61,80].

We have summarized the key attributes of slow earthquakes derived from seismological and geodetic and constructed a list of predicted geological characteristics that are developed from these data as a guide for identifying the signatures of slow earthquake deformation in ancient rocks for future geological investigations (Table 1).

[H1] Potential slow earthquake structures

In this section, we summarize observations of a selection of ancient, exhumed structures, which address some of the critical properties of slow earthquake sources that geological observations are well placed to help elucidate: the physical characteristics of potential slow earthquake structures (thickness, mechanical composition), the deformation mechanisms at the locus of slip, and the in situ effective stress conditions. To ensure the information is relevant to slow earthquakes generally, we synthesize observations from systems that were active across the range of tectonic settings shown in Figure 1 (locations shown in Figure 1, for details see

Supplementary Table 1). They include subduction plate boundary faults, upper plate faults at subduction zones, and transform faults. Throughout, we have attempted to identify only the features that formed at metamorphic conditions relevant to slow earthquakes, particularly where subsequent deformation or retrograde metamorphism occurred during exhumation[83]. We focus on structures that exhibit shear offset, consistent with geodetic and seismological observations. However, we have not precluded any features from within these systems in order to encompass as full a range of deformation structures as possible. For simplicity, we use the term 'plastic' to encompass grain-scale deformation by dislocation motion **[G]**, diffusion creep **[G], or** dissolution-precipitation creep unless otherwise stated.

[H2] Thickness of deformation zones

The maximum thickness of the exhumed structures is a constraint on the total thickness of zones that host slow earthquakes in modern systems. Geologically, the maximum thickness is approximated by zones of distributed shear deformation in which finite strain **[G]** is inferred to be higher than in the surrounding (background) rocks. These high strain zones have total observed thicknesses from tens of meters to as much as a few kilometers, lengths of kilometers to hundreds of kilometers, and contain brittle (FIG. 2A) or plastic (FIG. 2D) structures or both. Brittle elements that define distributed high strain zones include particulate or cataclastic flow **[G]**, zones of high vein density, anastomosing shear band networks (FIG. 2C), and mixing resulting in stratal disruption (FIG. 2A). Distributed shear deformation accommodated by plastic mechanisms is indicated by pervasive foliations **[G]** (FIG. 2D, F), folds, and associated kinematic indicators (FIG. 2F). Finite strain and inferred strain rates within high strain zones are

spatially variable, and presumably strain and strain rate patterns also varied over time during progressive deformation. Observed high strain zone thicknesses are upper bounds on active thicknesses as migration of deformation with time can result in total thicknesses greater than the zone that is deforming at any one time[84].

Relatively localized faults and shear bands with thicknesses ranging from sub millimeter to meters are ubiquitous within or at the edges of high strain zones[85] (FIG. 2C-F), suggesting strain is localized to varying degrees within individual deformation environments. The degree of localization varies within individual deformation environments such that there may be a continuum of structures with different thickness[86]. Although finite strain can rarely be measured, localized structures are generally inferred to have accommodated a greater component of shear displacement than their surroundings[87,88]. Relatively localized structures at the edges of high strain zones include out of sequence thrusts or thrusts at the base of nappes (FIG. 2C), which are typically continuous for kilometers along strike and accommodate the majority of offset across a system in a particular phase of deformation[43,89,90].

Within high strain zones, discrete, localized shear bands are common at all metamorphic grades and across a wide range of rock types (FIG. 2E, F). Individual bands are locally discordant to and deflect the surrounding foliations, though meters-long, submillimeter-thick, foliation-parallel bands are also observed[91]. Shear bands typically form anastomosing **[G]** networks, where both the width of the networks and the length of individual shear bands is at least meters to tens of meters, although the size of exposure limits observation beyond this minimum length scale[92] (an example network is shown in FIG. 3C). In predominantly plastic high strain zones, some shear

bands containing ultramylonite may be traced for kilometers[93,94]. Shear bands also define S-C-C' composite fabrics **[G]** in predominantly plastic shear zones, which are typically finer grained than the surrounding rock, suggesting they were relatively weak[86] and/or may represent deformation at higher strain rates[95-97]. Shear bands in composite fabrics tend to be centimeters to tens of centimeters long. Lengths of localized structures therefore range from 10^{-3} – 10^{-2} m (C-C' bands) to 10^{0} –10^{3} m (shear bands) or more if linkage of ultramylonite bands, faults, and shear zones occurs within structural complexes and nappe stacks. As strain rates were likely elevated in these shear bands compared to the surrounding rock, they may be candidate host structures of the transient increases in strain rate associated with slow earthquakes.

[H2] Heterogeneous mechanical components

Mechanical heterogeneity is thought to limit slow earthquake slip rates and potentially cause local variations in slip rate that result in LFEs[45,98]. Heterogeneity is inherent to all of the structures we reviewed, which contain assemblages of different rock types or components with different grain size, with, on average, aligned structural components. Field observations of boudinage or buckle folding **[G]** of relatively more competent units are common to all metamorphic environments, which demonstrate the different components had different effective viscosity under in situ conditions. Veins are also commonly boudinaged and folded.

High strain zones containing heterogeneous mechanical components are common in subduction zones. Mélange **[G]** zones developed at subduction zone plate boundaries at temperatures less than around 350 °C contain block-in-matrix fabric where blocks of relatively coarse grained

siliciclastic and mafic volcanic rocks are interspersed in a matrix of pelitic rock **[G]** (FIG. 3A). Similar assemblages are developed in faults cutting off-scraped units that were never buried deeply. These faults are defined by zones of stratal disruption in which coarser-grained layers are broken up and boudinaged within a pelitic matrix[99-102]. Rocks that were buried to greater depths in subduction systems experience additional disruption[103]. Deformation to greater strains at increasing temperatures involves additional folding and transposition **[G]** of layering, boudinage **[G]**, and imbrication **[G]**, which all further mix lithologies[39,104,105]. Lithologic heterogeneity is also characteristic of serpentinite-bearing shear zones on prograde deformation **[G]** paths or at peak conditions, where the degree of serpentinization may be spatially variable and in some cases serpentinite shear zones contain exotic blocks[40,106,107].

Exhumed continental transform faults also contain mixtures of lithologies due to transposition and boudinage, predominantly of more and less phyllosilicate-rich units[93,108,109]. Heterogeneous fault rocks also develop in single lithologic units due to variations in finite strain where blocks of relatively coarse grained protomylonite and weakly deformed protolith are surrounded by finer-grained mylonite or ultramylonite zones[86,93].

We compiled field data describing the characteristics of competent block in various high strain zones to determine if the populations of blocks are similar (FIG. 3). All block populations exhibit an apparent power-law distribution of sizes[110,111] (FIG. 3B). In addition, a power-law model is a plausible fit[112] for datasets with ~1000 measurements, though this cannot be evaluated for smaller datasets. Substantial variation is observed in the power law scaling exponent when exposure-scale measurements (10^{-2} – 10^{1} m, maximum observed dimension limited by exposure

size) are compared, reflecting heterogeneity within and between systems[110]. The largest-scale relatively competent lenses within mélange zones can be mapped for over 1 km (e.g. basaltic rocks at the base of a unit of mélange), representing a potential upper bound on block size. Block long axes have a preferred orientation clustered around the high strain zone boundaries (±15 °) (FIG. 3C). More elongate, higher aspect ratio blocks are less common than more equant blocks (FIG. 3D) so that the populations have log-normal axial ratio distributions[111]. Comparison of mélanges that formed at different temperatures (Lower and Upper Mugi and Makimine mélanges, Cycladic Blueschist Unit) suggests the blocks may be progressively broken down into smaller units during underthrusting, though the range of aspect ratios is similar[39,111]. Lithologically distinct or low strain blocks within the Kuckaus continental transform zone[93], show a similar distribution of aspect ratios, range of block dimensions (with the largest over 2 km), and clustering of long axis orientations (±16 °) as the subduction mélange examples.

[H2] Deformation mechanisms

Analysis of ancient structures is the only way to directly evaluate the grain-scale deformation mechanisms that are important in environments that host slow earthquakes. A variety of grain-scale deformation mechanisms were active in the exhumed structures, but they all have one thing in common: deformation was accommodated by a combination of syn-tectonic plastic and brittle mechanisms (FIG. 4). In subduction zone faults and accretionary wedge thrusts at temperatures less than ~350 °C, the predominant plastic deformation mechanism is dissolution-precipitation creep in rocks containing quartz and clay minerals[111,113,114] (FIG. 4A, B). Higher-temperature subduction and transform structures exhibit evidence for a range of plastic deformation

mechanisms, including both dislocation creep[39,115] **[G]** and diffusion creep[86] **[G]**) in foliation-defining phases such as quartz and calcite, or amphiboles in some mafic rocks (FIG. 4C). Plastic deformation mechanisms result in the penetrative foliations (FIG. 4A-D) and grain shape preferred orientations (FIG. 4 C) that define both the maximum widths of the high strain zones and localized shear bands (FIG. 4 D).

Structures that form by fracture and frictional sliding contemporaneously with plastic deformation occur at a range of scales. The discrete, localized structures at the boundaries of high strain zones are typically brittle structures[89,90]. High strain zones representative of both low and high temperature systems contain localized shear bands (FIG. 2B), cataclasitic bands **[G]** (FIG. 4A), breccias (FIG. 4E) and, in some cases, pseudotachylytes **[G].** Where present, these localized structures commonly form at the interfaces between units of different competence[108,116,117] and along foliations[116,118,119]. Veins are common to most of the exhumed high strain zones, typically occurring in discrete sets either parallel or discordant to penetrative foliations (FIG. 4F, G). Grain-scale brittle deformation is a fundamental mechanism in phyllosilicates, which are foliation-defining phases in many cases (FIG. 4A, B, D). Microcracking (and/or veining) of the crystal lattice is accompanied by kinking, dislocation glide along basal planes[95,120], and recrystallization by a dissolution-precipitation mechanism, resulting in a penetrative semibrittle behavior[40,41,95,120-122]. Grain-scale brittle deformation in phyllosilicate rich rocks, along with the zones of stratal disruption in shallow subduction zone or accretionary wedge faults where particulate flow may have predominated[99], can result in meters or tens of meters-wide deformation zones. However, discrete brittle structures (with thicknesses of the order of millimeters or centimeters) are generally relatively localized while structures resulting from crystal-plastic deformation are always more distributed.

Mutually crosscutting relations between fractures, best recorded by veins, and surrounding foliations are the primary evidence for fracture and plastic deformation occurring contemporaneously[123] (FIG. 4F). Veins that were boudinaged, folded and/or exhibit evidence for plastic grain-scale mechanisms[37,40,124] underwent some plastic deformation after formation. Repetition of this pattern, indicated by crosscutting veins, foliation wrapping around boudinaged veins while other veins crosscut the foliation, and veins that record different finite strain subsequent to formation indicate fracture and viscous deformation occurred cyclically[123,125,126]. In the structures we reviewed, veins are far less common in transform faults than in subduction systems. However, some transform faults preserve brittle deformation in the form of pseudotachylyte slip surfaces[119,127] and associated breccias[128] (FIG. 4E), which are subsequently folded or show evidence of grain-scale plasticity. The inferred cyclicity between localized fracture and distributed plastic deformation is consistent with the seismological and geodetic observations of slip at different slip rates at the same place on active structures hosting slow earthquakes.

[H2] Fluid pressure and effective stress

Tomographic images of seismic velocity in systems such as the Cascadia[76,129], Mexico[73], and Nankai[75] subduction zones, among others, indicate that slow earthquakes occur at high pore fluid pressure and low effective stress. Geological constraints on effective stresses could verify these observations and test if they are generally applicable. However, field-based estimates of effective stresses are available for only a few exceptional systems, such as the Makimine mélange (Japan)

and Chrystalls Beach mélange (New Zealand), which exhibit well-defined vein geometrical relations and kinematics that constrain the effective stress for frictional slip. Elsewhere, stress conditions can only be inferred by comparison to lab-derived flow laws through empirical relations between steady-state flow stress and grain size during dislocation creep (paleopiezometry)[130]. The available data suggest shear offset does occur under elevated pore fluid pressure (greater than hydrostatic, approaching lithostatic) and low effective normal stress conditions (differential stress of the order of 1 to 10 MPa)[37,131]. Though absolute measures of effective stress are rare, similarities in vein network characteristics in multiple systems suggests a similar conclusion is appropriate for many of the exhumed structures[39,125,130].

Field- and micro-scale constraints on vein opening vectors demand the occurrence of tensile failure at the depths and conditions of slow earthquakes[37,40,131]. These veins are interpreted to form as opening-mode extensional hydrofractures. Extensional fractures can accommodate shear offsets when arranged in an en echelon **[G]** geometry, which are documented in some serpentinite shear zones[106] and high temperature subduction shear zones[36,37,125]. Such en echelon shear zones are generally up to a few meters wide and traceable for meters to tens of meters, generally constrained by outcrop continuity.

Veins or mineralized faults with confirmed shear offsets, which indicate shear failure under elevated pore fluid pressure conditions, are observed in some high strain zones. In subduction mélanges, shear-offset veins occur along shear bands and parallel to solution cleavages throughout the matrix, while extensional veins form discordant to the cleavages[36,37,92]. The kinematics and attitudes of the two vein sets combined with failure criteria for the anisotropic

rocks[133] suggest slip at differential stress of ~1 MPa and elevated pore fluid pressure (approaching lithostatic values)[37,131]. The low differential stress reflects the preference of tensile over shear failure. However, tensile veins are typically filled by a relatively competent quartz precipitate, which is easily preserved and recognized, whereas discrete shear surfaces can easily be overprinted in environments of efficient plastic deformation. Therefore, it is possible that the dominantly extensional vein systems were accompanied by substantial but undocumented shear failure. Similar vein sets, vein attitudes with respect to foliation, shear offsets across foliation-parallel veins, and inferences regarding rock mechanical anisotropy are documented in a variety of subduction mélanges[92,125] and accretionary wedge thrusts[134], suggesting that these low effective stress conditions may be commonly achieved.

Small differential stresses are also inferred from structures in which plastic deformation was predominant by extrapolating flow laws and stress-grain size relationships to in situ conditions[130]. Downdip of the seismogenic zone in subduction zones, deformation at ~500-600 °C partitioned into biotite-rich layers at plate rates to SSE slip rates requires shear stresses of the order of 1-10 MPa[125]. In quartzofeldspathic rocks typical of continental transform faults, flow stresses within high strain zones at 450-480 °C are on the order of 30 MPa or less, as calculated from quartz piezometry and corrected for bulk rock composition[86]. Flow laws are not well defined for some mineral phases (e.g. amphiboles), but strain is distributed across both mafic and silicic or calcic rocks in high strain zones at blueschist to eclogite conditions, indicating all lithologies were relatively weak[39]. Vein formation during predominantly plastic deformation at higher temperature also indicates near-lithostatic pore fluid pressures[39,43,135]. Overall, the geological observations suggest slow earthquake deformation in the deep extents of active

systems occurs at differential stress that is a small fraction of the lithostatic load, potentially accompanied by large pore fluid pressure.

Cycling of stress magnitudes, orientations and/or pore pressures is inferred from repetitive fracture during contemporaneous fracture and crystal-plastic deformation[37,40,43,90,123]. Incremental shear offsets of around 10-100 μm across foliation-parallel veins (FIG. 4G) combined with vein lengths of the order of 1-10 m, have been used to infer stress drops of tens of kPa, comparable to those determined seismologically for individual LFEs, accompanied by pore pressure drops[36,123]. Plastic deformation in the rock surrounding these veins accommodated some strain in the times between slip increments. Foliation-parallel shear veins in the same exposures as foliation-parallel extensional fractures indicate cyclical switching between the maximum and minimum compressive principal stresses, consistent with small differential stresses and pore pressure cycling[37,124]. Repetitive fracture, stress field rotations, and alternating brittle and plastic deformation are also evidenced by veins in mutually crosscutting sets parallel and discordant to the foliation, within which older veins are folded and/or boudinaged[39,123].

[H 1] Picture of a slow earthquake source

The large range of conditions and locations in which slow earthquakes are observed seismologically (FIG. 1A) requires that no single mineral phase, lithology, or metamorphic reaction controls slow earthquake slip. This observation implies that slow earthquake phenomena arise from some combination of loading and in situ conditions[42], which can develop and generate similar seismological signals in a large variety of settings.

Some features are common to all of the apparently diverse structures reviewed in the previous section, which we suggest can be used to develop a general picture of a slow earthquake source in any tectonic environment. Our review suggests the host structure comprises a high strain zone from at least tens of meters to kilometers in total thickness that accommodates shear displacement, but which also contains more localized, typically anastomosing, millimeter- to centimeter-thick shear-offset structures. Within the high strain zone, coeval plastic (intracrystalline and/or diffusive mass transfer) and brittle (fracture, frictional sliding granular/cataclastic flow) deformation mechanisms result in mutually crosscutting continuous and discontinuous structures. The high strain zone contains a heterogeneous assemblage of lithologies and/or components with length scales from centimeter to kilometer that have variable competency under in-situ conditions. A well-defined foliation is present throughout the high strain zone defined by compositional layering and/or mineral grains with shape-preferred orientations, which result in mechanical anisotropy facilitating frictional failure along weak planes. The foliation contains aligned grains of mineral phases that are intrinsically weak or promote deformation at low differential stress under in situ conditions, regardless of the deformation mechanism. Deformation resulting in slow earthquakes is fluid assisted and likely occurs at high pore fluid pressures.

Considered individually, each of the characteristics listed above could apply to many ancient faults and shear zones and none of them *require* deformation at slip rates corresponding to slow earthquakes. Therefore, none of these common characteristics can be considered a definitive indicator of slow earthquakes in the rock record. As the grain-scale deformation mechanisms

must be variable throughout the crust, a wide variety of structures might have accommodated slow earthquakes, and structures that were active in different tectonic settings may have different characteristics in exposure.

[H21] Unravelling slip rates

In the absence of a single, universal deformation structure or mechanism diagnostic of slow earthquake slip rates, how can the fingerprint of slow earthquakes be recognized in the rock record? One approach is to distinguish the relative slip or strain rates associated with categories of structures within exhumed high strain zones that contain multiple styles of deformation (e.g. distributed and localized), but which developed in the same phase of deformation. If the structural elements that require aseismic (plate motion, i.e. $\leq 10^{-9}$ ms^{-1}) or regular seismic rates ($\sim 10^{0}$ ms^{-1}) can be identified, then any other structures may have formed at intermediate rates and be candidates for accommodating slow earthquakes[136].

For example, in the lower Mugi mélange in the Shimanto Belt, Japan, pseudotachylytes and fluidized cataclasites in the unit-bounding thrusts record seismic slip rates and potentially large-magnitude earthquakes[89,113]. The pervasive cleavage distributed throughout the pelitic matrix of the mélange formed by dissolution-precipitation creep in quartz, which is rate limited by the slowest of dissolution, diffusion, or precipitation of silica. The constitutive relations for dissolution-precipitation creep[137] (FIG. 5) suggest that for a grain size of around 10 μm, representative of the pelitic matrix, slip rates characteristic of both plate motions and SSEs can be accommodated by dissolution-precipitation creep within shear zones of the order of 10 cm

438 thick if the mechanism is dissolution limited and millimeters thick if the mechanism is diffusion
439 limited[138]. Zones at least a few centimeters-thick of higher shear strain with mutually
440 crosscutting relations with the surrounding solution cleavage may therefore be a potential record
441 of geodetically observed slow slip[37]. However, seismologically observed slow earthquakes with
442 slip rates of millimeters per second cannot be accommodated by dissolution-precipitation creep
443 under these conditions unless the thickness of a continuous shear zone is tens of meters or more,
444 suggesting they require an alternative process[138].
445
446 The remaining structures within the mélange, which might have hosted ancient seismologically
447 observed slow earthquakes, are the phyllosilicate-rich shear band-vein networks distributed
448 throughout the pelitic matrix and cataclastic bands identified at matrix-block margins. There are
449 no lower or upper bounds on slip rate for these two features so they may have accommodated the
450 whole range of tectonic slip rates[139]. It is also possible that the full range of tectonic slip rates
451 could have been hosted by the through-going, bounding thrusts[136], and the evidence for slow
452 earthquake slip rates was either overprinted, unrecognized, or is indistinguishable. However, this
453 analysis suggests mutually crosscutting structures with a range of inferred slip rates within one
454 system may be the nearest thing to a signature for slow earthquakes[136,140,141].
455
456 ***[H2] Geometry of slow earthquake sources***
457
458 We present a conceptual model of a slow earthquake source structure in Figure 6, which
459 illustrates the geometry and spatial relations of shear-offset structures that slip at different rates
460 within a single system. Figure 6 depicts the cross-sectional area of a high strain zone roughly

comparable to the source region of an LFE family[49]. Drawing on the inferences made previously for the Mugi mélange, as representative of the subduction mélanges we reviewed, this model suggests slow slip events (SSE) might be accommodated by zones of matrix a few to tens of centimeters thick between blocks, which are common within the mélange, or across thicker shear zones containing both matrix and blocks[142]. Shear band-vein networks and cataclastic bands exist in interconnected networks that are continuous for at least tens of meters, and must extend farther than this lower bound[92]. A moderately large LFE source may therefore consist of an anastomosing fault, shear band and/or vein network rather than a single planar fault surface. Non-coplanar shear structures are prevalent, raising the possibility of synchronous slip across multiple subparallel surfaces. Competent block margins are commonly aligned with the shear bands, supporting the inference that the mechanical contrast at the interfaces between relatively competent bodies in a weak matrix, where stress is amplified and/or frictional stability or rock permeability vary, are central to strain localization[143,144]. Due to their non-planar geometry, any slip across a single band or network of bands would cause heterogeneous loading of the surrounding rock volume.

We suggest the model shown in Figure 6 is representative of slow earthquake source structures across the metamorphic environments of slow earthquakes (FIG. 1). Though the lithologies and active deformation mechanisms differ, the mechanical heterogeneity, thicknesses, and geometries of structures associated with different strain rates, and the inferences regarding effective stress conditions are similar for all the structures we reviewed. A key insight is that available mineral flow laws suggest that geodetically observed slow earthquakes may be accommodated by commonly identified ductile shear zones in many exhumed structures at low

differential stress (~1-10 MPa) under the in situ conditions of deformation[39,125,130]. Rather than representing steady-state creep, slow earthquake slip would then occur through episodic increases in stress or decreases in strength[145]. This is permissible, but not required by, the geological observations. For example, geodetically observed slow earthquakes could also be accommodated by small increments of slip across isolated structures or through linkage of parallel but non-coplanar segments of shear-vein networks.

Within high temperature, predominantly plastic high strain zones, relatively localized shear-offset structures, which might be candidate LFE hosts, fall into two broad categories: vein networks and shear bands. The rates at which veins form are not well constrained, but the kinematics of vein-filled fractures and the association with rigid blocks are consistent with seismologically observed slow earthquake occurrence[39,135]. Ultramylonite **[G]** shear bands are displacement discontinuities within predominantly plastic high strain zones[87]. Available flow laws suggest millimeter-thick ultramylonite shear bands are too thin to accommodate slow earthquakes. However, thicker ultramylonite bands are documented[93,108] and overall have similar geometries to shear band networks in low temperature mélanges[93]. Further investigation is necessary to establish the deformation mechanisms active within plastic shear bands and to investigate whether those mechanisms can accommodate strain at low flow stress compared to the remotely applied stress[146], can accommodate strain rates high enough to result in geodetically detectable strain rate transients or radiated seismic energy.

[H1] Mechanisms of slow earthquakes

A variety of modeling studies have proposed mechanisms that explain how slip on a fault might occur relatively slowly rather than manifesting as seismic slip. Several of the mechanisms rely on specific frictional behavior of the materials at the sliding interface[147]. In the framework of rate and state friction, slow slip is predicted when the fault system stiffness approaches the critical stiffness for instability[148,149], which is promoted by low effective normal stress and near velocity-neutral frictional stability[149]. Slow slip is also possible when a fault exhibits a transition from velocity-weakening to velocity-strengthening at a slip speed larger than the plate convergence rate[150-152]. Dilatant strengthening, where dilatancy during slip reduces pore pressure and prohibits a transition to full instability, has been proposed as a potential mechanism that limits the slip rate[153,154]. Geometric complexity on a fault with uniform velocity-weakening behavior has also been shown to result in slow slip[155].

Geological observations can determine which of these mechanisms may be important in specific settings. For example, pelitic rocks are likely present in high strain zones that host slow earthquakes in the shallow portions of subduction zones. Lab experiments show pelitic rocks have near velocity-neutral frictional stability and exhibit a transition from velocity-weakening to velocity-strengthening behavior with increased velocity[32,156,157]. Serpentinite, inferred to be common near the mantle wedge corner coincident with the locus of slow earthquakes in some subduction zones[73], also shows a change from velocity-weakening to –strengthening at increasing velocity[158]. Competent blocks of basalt in mélanges have been shown to be velocity-weakening[117] suggesting that slip zones that mix clay and altered basalts might favor slow slip[117,145,159]. Furthermore, the anastomosing geometry of shear band-vein networks and cataclastic bands might be fundamental to generating slow slip across many environments[107,155].

These observations therefore suggest that the frictional behavior of the materials in the high strain zones, the intrinsic heterogeneity of the high strain lithologic components, and the geometry of potential slow earthquake structures all contribute to generating the spectrum of slow slip rates.

Our review suggests that in all metamorphic environments, the combination of frictional sliding and plastic grain-scale deformation mechanisms is essential to slow earthquake deformation. Systems characterized by coupled frictional and plastic mechanisms are expected to exhibit spatially continuous and strain-rate dependent, temporally transient deformation[121,137]. The emergence of transients comparable to slow slip events in dry rock friction experiments at room temperature[32-34,148] indicates that phenomena similar to slow earthquakes can result from purely frictional processes. In the structures we reviewed, frictional sliding at temperatures less than ~350 °C was accompanied by dissolution-precipitation creep (FIG. 4A), which forms solution cleavages perpendicular to the shortening direction during deformation. This plastic component of the deformation may therefore enhance the tendency for slow slip by accommodating compaction, leading to reduced porosity and elevated pore pressure with time. Dissolution-precipitation creep may also increase the real area of frictional contacts, causing the state variable to evolve with time[160] and potentially acting as an advanced healing mechanism to promote stable accelerating slip[32].

The controls on slow slip in higher-temperature systems, where plasticity rather than frictional sliding is predominant, are less clear. During deformation accommodated by plastic grain-scale mechanisms, instability and a transition to high strain rate transients or frictional sliding can

occur in a phenomenologically similar way to rate and state frictional behavior[161]. The transition is generally promoted by stress heterogeneity[162], strain hardening, and/or pore pressure cycling[163]. Strain hardening is inherent to foliation-defining phases such as phyllosilicates (FIG. 4D, E), in which recovery is limited under in-situ conditions, as evidenced by kinking at grain to exposure scales[41,95]. Rocks dominated by phyllosilicates are also considered to be low permeability[164-167], so likely important to maintaining high pore fluid pressures, and can cause pore pressure changes by dehydration and/or metamorphic reactions[40,168]. The onset of instability may therefore be controlled by the balance between strain hardening and the efficacy of recovery mechanisms during a perturbation to steady state conditions[162,169]. Further work is needed to examine predominantly plastic systems to determine whether there is a condition for stable accelerating slip for plastic deformation.

Future Perspectives

In this Review, we selected ancient structures exhumed from the range of tectonic settings and P-T conditions illustrated in Figure 1 as possible examples of those hosting active slow earthquakes. We focused our selection by noting that shear offset is required at the slow earthquake source, which must be recorded in the deformation structures. The characteristics identified as common to slow earthquakes (FIG. 6) are common in exhumed crustal faults, so could be considered too generalized to be useful, though this may also simply reflect that slow earthquakes are a common phenomenon. Observations of slow earthquakes increase continually. Combined with the recognition of pre- and afterslip associated with many earthquakes and long-term, low strain rate transients in some systems[8], we suggest slip rates (10^{-10} – 10^{-3} ms^{-1}) and

575 strain rates (10^{-10} – 10^{0} s^{-1}) intermediate between seismic (>10^{-0} s^{-1}) and plate-rate creep (10^{-14} –
576 10^{12} s^{-1}) should be common to many fault zones, even if they appear to lack conspicuous
577 evidence for slow slip.
578
579 We have not found a conclusive indicator of slow earthquake slip rates in the exhumed systems
580 we reviewed so we cannot independently confirm if these systems actually hosted slow
581 earthquakes. Additionally, there may be other structures that we have not considered here that
582 could host slow earthquakes, so the list of slow earthquake characteristics should not be
583 considered exhaustive. For example, centimeter-thick layers of foliated cataclastic rocks in
584 localized structures that exhibit evidence for seismic slip have been inferred to record slow slip
585 rates[136]. However, this association was inferred following a similar approach outlined here for
586 the Mugi mélange, by identifying different structures that might correspond to distinct strain and
587 slip rates within a system that deformed in an equivalent setting to where slow earthquakes are
588 observed. More work is needed to determine the scales of observation at which the variations in
589 slip rate can be inferred in a broad range of systems.
590
591 Overall, good agreement between the slow earthquake characteristics predicted from geophysical
592 observables (Table 1) and the systems we reviewed indicates the structures we reviewed are
593 good candidates as hosts of slow earthquakes. In particular, the thickness of the high strain zones
594 (of the order of 10^{1} to 10^{3} m), and maximum dimension (~10^{2} to 10^{3} m) and apparent power law
595 distribution of sizes of rheological heterogeneities limited by the shear zone thickness, are
596 comparable to LFE size distributions[48,170,171]. Geological evidence supports deformation at low
597 differential stress, generally <10% of the lithostatic load, and high pore pressure, in some cases

approaching lithostatic[37,131]. A major limitation to these stress estimates is the limited availability of flow laws for the relatively incompetent, foliation-defining phases that are generally accepted as important in accommodating simple shear (e.g. phyllosilicates and amphiboles).

Further investigations of the possible geological structures that host slow earthquakes, within and across their tectonic and metamorphic settings, are essential to the future of slow earthquake science. The defining characteristic of slow earthquakes is that they are slow. Field and microstructural observations are uniquely able to identify the controls on slow earthquake slip rates, slip amounts, and spatial relations between slip at different rates, and therefore explain why slow earthquakes are distinct from regular earthquakes. If a slip rate-limiting mechanism could be identified, the deformation structures or textures it produces may be diagnostic of slow earthquakes in the rock record. Increases in porosity due to dilatant strengthening[153,154], which is one candidate limiting mechanism, may cause fluctuations in pore fluid pressure within a slow earthquake slip zone and could result in mineral precipitation that is preserved as veins. Enhanced porosity is a potentially generic process to all slow earthquakes, so mapping veins or grain-scale mineralization to evaluate this model is an important avenue for future research. Even if a universal rate-limiting mechanism can be established, geological observations emphasize that experimental and theoretical studies are needed to resolve how the spectrum of slow earthquake slip rates can arise from different grain-scale deformation mechanisms.

One challenge for geologically-focused work is to extrapolate exposure- or micro-scale observations to length scales relevant to slow earthquake processes. In particular, a major outstanding issue is the cause of observed rates of tremor migration and reversals[82]. Geological

observations need to reconcile the length scales over which these migration patterns develop with the variability in rock type and structural assemblage observed in typical outcrops. Current and future geological interpretations could be tested by better source time functions for LFEs, improved hypocentral locations of LFEs and detailed evaluation of focal mechanism variability to compare to the geometry of anastomosing networks of shear bands.

Slow earthquake geology is a new frontier in studies of fault and shear zone rocks. Reinterpretation of deformation structures is necessary in light of the geophysical documentation of transient increases in slip and strain rates associated with slow earthquakes in a wide range of tectonic settings. With this perspective, studies of exhumed analog structures from across the range of metamorphic and tectonic settings of slow earthquakes can inform the physical controls on slow earthquakes, which is central to understanding of plate boundary fault and shear zone mechanics.

Author contributions:

All authors contributed to the researching of data and writing of the manuscript and to the discussion of the content.

Acknowledgements: We thank Yujin Kitamura and Alissa Kotowski for providing data for Figure 3B and Noah Phillips and Alissa Kotowski for providing photomicrographs in Figure 4A, and 4c, respectively. Thanks also to Alissa Kotowski, Christie Rowe, and Randy Williams for discussions and feedback on an early draft of the manuscript. This work was supported by the Natural Sciences and Engineering Research Council of Canada (NSERC), Discovery Grant

RGPIN-2016-04677 (JK), the European Research Council (ERC) under the European Union's Horizon 2020 research and innovation programme, Starting Grant agreement 715836 (AF), and the Earthquake Hazards Program of the U.S. Geological Survey (DS).

Competing interests: Authors declare no competing interests.

Correspondence and requests for materials should be addressed to James Kirkpatrick

james.kirkpatrick@mcgill.ca

Key points (30 words)

- The global distribution and pressure-temperature range of seismologically observed slow earthquake hypocenters implies no single mineral phase, lithology, or metamorphic reaction controls slow earthquake slip.
- No single, universal deformation structure or deformation mechanism is a clear indicator of slow earthquakes in the rock record. Multiple different mechanisms or combinations of mechanisms can produce the same macroscopic behaviors.
- A seismologically observed slow earthquake source may consist of an anastomosing fault, shear band, and/or vein network (potentially including synchronous slip across multiple sub-parallel surfaces) rather than a single planar fault surface.
- Geodetically observed slow earthquakes may be accommodated by commonly identified ductile shear zones in many exhumed structures
- Overall, the geological evidence suggests material heterogeneity, geometric complexity, and deformation at low differential stress are common to slow earthquake sources.

Glossary

Accretionary wedge: the accumulated rock scraped off the oceanic plate and transferred to the upper plate at subduction margins. These accumulations form a wedge shape in cross section.

Anastomosing: term used to describe a geometry in which surfaces or strands diverge and re-join, braided

Boudinage: process by which relatively competent layers split apart into smaller sections when stretched during extension. The surrounding relatively incompetent material deforms to accommodate the change in shape of the competent layer.

Buckle folding: folding that is inferred to form by layer-parallel shortening when relatively competent, or viscous, layers or features are surrounded by less competent rock.

Cataclastic flow: a brittle process in which a volume of rock deforms by frictional sliding and grain rolling combined with fracture, causing an overall change in shape.

Cataclastic band: Layer of fault rock in which the grain size is reduced due to cataclastic processes when the laeyr accommodated shear displacement

Composite fabric: foliation that is defined by more than one set of oriented fabrics in the rock, which form discrete sets.

Critically stressed fault: when the shear stress resolved on a fault is just below the frictional strength of the fault. The fault is then sensitive to small perturbations to the stress field as a small increase in shear stress can cause failure.

Crystal-plastic deformation: term referring to the intragranular deformation mechanisms that involve mechanisms that cause individual grains to change shape by dislocation-based mechanisms.

690 **Décollement**: the thrust fault that separates rocks transported in opposite directions.
691 Décollements are typically the most laterally continuous and the structurally lowest faults in a
692 system. Synonyms include detachment, basal fault.
693 **Diffusion creep**: a grain-scale deformation mechanism in which grains accommodate strain by
694 the diffusion of point defects through their crystal lattice.
695 **Dislocation creep**: intra-crystalline deformation mechanism in which strain is accommodated by
696 migration of dislocations, linear imperfections in the crystal lattice of grains, accompanied by
697 dislocation climb, a mechanism by which dislocations can move out of plane.
698 **Dislocation motion**: used here to refer to deformation mechanisms that involve movement of
699 dislocations, linear imperfections in the crystal lattice of grains, to accommodate strain.
700 **Double couple source mechanism**: The idealized fault plane model for an earthquake whose
701 displacement is within the plane of the fault, with both sides moving equal, opposite distances.
702 **En echelon**: describes the geometry of parallel or subparallel overlapping structures (usually
703 opening mode veins or faults) that are offset from one another in the direction perpendicular to
704 their long axes, and are oblique to the overall structural trend.
705 **Extensional hydrofracture**: opening mode cracks, formed when pore fluid pressure exceeds the
706 minimum compressive principal stress and the differential stress is less than twice the cohesion
707 of the rock.
708 **Foliation**: A rock fabric that can be approximated as a plane, often defined by the preferred
709 orientation of mineral grains and/or by compositional banding.
710 **Finite strain**: the total strain, or change in shape, that has affected a rock.
711 **Frictional sliding**: Displacement between two surfaces in contact, which is resisted by a shear
712 force proportional to the normal stress on the surface.

Hypocenter: the point on a fault where an earthquake rupture starts.

Imbrication: process of thrust faulting that causes multiple approximately parallel slices of rock to be thrust on top of one another.

Isoclinal folding: when a layer or planar feature is folded such that the fold limbs are close to parallel so that the layer seems to have been completely bent back on itself.

Mélange: mixtures of rock types that are characterized by a block in matrix fabric. Here used to refer to rock units that formed and deformed due to tectonic shearing.

Pelitic rocks: rocks that have a high clay content, and their metamorphic equivalents.

Phyllosilicates: minerals that are made up of stacks of parallel sheets of silicate tetrahedra, which are weakly bonded together. The phyllosilicates include clays and micas.

Pseudotachylyte: the quenched remnants of a molten rock that formed by frictional heating on a fault surface during earthquake slip. Used elsewhere to include impact-related melts.

Prograde deformation: Deformation that occurs while the rocks experience an increase in temperature and/or pressure, typically during burial (including subduction-related burial).

Protolith: the pre-deformation or pre-metamorphic equivalent of a deformed or metamorphosed rock.

S-C-C' composite fabric: a composite fabric consisting of more than one foliation that forms inside shear zones that deformed predominantly by plastic deformation mechanisms. The S-foliation represents deformation due to local shortening in the rock. C and C' foliations are small-scale shear bands within a larger shear zone. The angles between the foliations decrease with strain and the foliations can be difficult to distinguish.

Transposition: process by which rotation of layers during isoclinal folding or shearing causes the original orientation, angular relationships, and distinct features of the layers in the rock to be almost completely obliterated.

Tectonic tremor: low amplitude seismic signals defined by non-impulsive arrivals, similar to noise but distinguished by coherence over large geographic areas.

Ultramylonite: very fine-grained fault rock that deformed predominantly by plastic mechanisms.

References

1 Peng, Z. G. & Gomberg, J. An integrated perspective of the continuum between earthquakes and slow-slip phenomena. *Nature Geoscience* **3**, 599-607, doi:10.1038/ngeo940 (2010).

2 Obara, K. Nonvolcanic deep tremor associated with subduction in southwest Japan. *Science* **296**, 1679-1681, doi:10.1126/science.1070378 (2002).

3 Shelly, D. R., Beroza, G. C. & Ide, S. Non-volcanic tremor and low-frequency earthquake swarms. *Nature* **446**, 305-307, doi:10.1038/nature05666 (2007).

4 Rogers, G. & Dragert, H. Episodic tremor and slip on the Cascadia subduction zone: The chatter of silent slip. *Science* **300**, 1942-1943, doi:10.1126/science.1084783 (2003).

5 Ito, Y., Obara, K., Shiomi, K., Sekine, S. & Hirose, H. Slow earthquakes coincident with episodic tremors and slow slip events. *Science* **315**, 503-506, doi:10.1126/science.1134454 (2007).

6 Gomberg, J., Wech, A., Creager, K., Obara, K. & Agnew, D. Reconsidering earthquake scaling. *Geophys. Res. Lett.* **43**, 6243-6251, doi:10.1002/2016gl069967 (2016).

7 Frank, W. B. & Brodsky, E. E. Daily measurement of slow slip from low-frequency earthquakes is consistent with ordinary earthquake scaling. *Science Advances* **5**, doi:10.1126/sciadv.aaw9386 (2019).

8 Jolivet, R. & Frank, W. B. The Transient and Intermittent Nature of Slow Slip. *AGU Advances* **1**, e2019AV000126, doi:https://doi.org/10.1029/2019AV000126 (2020).

9 Ito, Y. & Obara, K. Very low frequency earthquakes within accretionary prisms are very low stress-drop earthquakes. *Geophys. Res. Lett.* **33**, doi:10.1029/2006gl025883 (2006).

10 Obana, K. & Kodaira, S. Low-frequency tremors associated with reverse faults in a shallow accretionary prism. *Earth and Planetary Science Letters* **287**, 168-174, doi:10.1016/j.epsl.2009.08.005 (2009).

11 To, A. *et al.* Small size very low frequency earthquakes in the Nankai accretionary prism, following the 2011 Tohoku-Oki earthquake. *Phys. Earth Planet. Inter.* **245**, 40-51, doi:10.1016/j.pepi.2015.04.007 (2015).
12 Kao, H. *et al.* A wide depth distribution of seismic tremors along the northern Cascadia margin. *Nature* **436**, 841-844, doi:10.1038/nature03903 (2005).
13 Shaddox, H. R. & Schwartz, S. Y. Subducted seamount diverts shallow slow slip to the forearc of the northern Hikurangi subduction zone, New Zealand. *Geology* **47**, 415-418, doi:10.1130/g45810.1 (2019).
14 Todd, E. K. *et al.* Earthquakes and Tremor Linked to Seamount Subduction During Shallow Slow Slip at the Hikurangi Margin, New Zealand. *J. Geophys. Res.-Solid Earth* **123**, 6769-6783, doi:10.1029/2018jb016136 (2018).
15 Toh, A., Obana, K. & Araki, E. Distribution of very low frequency earthquakes in the Nankai accretionary prism influenced by a subducting-ridge. *Earth and Planetary Science Letters* **482**, 342-356, doi:10.1016/j.epsl.2017.10.062 (2018).
16 Ito, Y. & Obara, K. Dynamic deformation of the accretionary prism excites very low frequency earthquakes. *Geophys. Res. Lett.* **33**, doi:10.1029/2005gl025270 (2006).
17 Aiken, C. *et al.* Exploration of remote triggering: A survey of multiple fault structures in Haiti. *Earth and Planetary Science Letters* **455**, 14-24, doi:10.1016/j.epsl.2016.09.023 (2016).
18 Peng, Z. G. *et al.* Tectonic Tremor beneath Cuba Triggered by the M-w 8.8 Maule and M-w 9.0 Tohoku-Oki Earthquakes. *Bulletin of the Seismological Society of America* **103**, 595-600, doi:10.1785/0120120253 (2013).
19 Chao, K. & Obara, K. Triggered tectonic tremor in various types of fault systems of Japan following the 2012 M(w)8.6 Sumatra earthquake. *J. Geophys. Res.-Solid Earth* **121**, 170-187, doi:10.1002/2015jb012566 (2016).
20 Gomberg, J. *et al.* Widespread triggering of nonvolcanic tremor in California. *Science* **319**, 173-173, doi:10.1126/science.1149164 (2008).
21 Chao, K. *et al.* A Global Search for Triggered Tremor Following the 2011 M-w 9.0 Tohoku Earthquake. *Bulletin of the Seismological Society of America* **103**, 1551-1571, doi:10.1785/0120120171 (2013).
22 Wang, T. H., Cochran, E. S., Agnew, D. & Oglesby, D. D. Infrequent Triggering of Tremor along the San Jacinto Fault near Anza, California. *Bulletin of the Seismological Society of America* **103**, 2482-2497, doi:10.1785/0120120284 (2013).
23 Scarpa, R. *et al.* Slow earthquakes and low frequency tremor along the Apennines, Italy. *Annals of Geophysics* **51**, 527-538 (2008).
24 Wech, A. G. & Creager, K. C. A continuum of stress, strength and slip in the Cascadia subduction zone. *Nature Geoscience* **4**, 624-628, doi:10.1038/ngeo1215 (2011).
25 Araki, E. *et al.* Recurring and triggered slow-slip events near the trench at the Nankai Trough subduction megathrust. *Science* **356**, 1157-1160, doi:10.1126/science.aan3120 (2017).
26 Kato, A. *et al.* Propagation of Slow Slip Leading Up to the 2011 M-w 9.0 Tohoku-Oki Earthquake. *Science* **335**, 705-708, doi:10.1126/science.1215141 (2012).
27 Wallace, L. M. *et al.* Slow slip near the trench at the Hikurangi subduction zone, New Zealand. *Science* **352**, 701-704, doi:10.1126/science.aaf2349 (2016).
28 Veedu, D. M. & Barbot, S. The Parkfield tremors reveal slow and fast ruptures on the same asperity. *Nature* **532**, doi:10.1038/nature17190 (2016).

29 Obara, K. & Kato, A. Connecting slow earthquakes to huge earthquakes. *Science* **353**, 253-257, doi:10.1126/science.aaf1512 (2016).
30 Kano, M., Kato, A. & Obara, K. Episodic tremor and slip silently invades strongly locked megathrust in the Nankai Trough. *Scientific Reports* **9**, doi:10.1038/s41598-019-45781-0 (2019).
31 Behr, W. M. & Burgman, R. What's down there? The structures, materials and environment of deep-seated slow slip and tremor. *Proceedings of the Royal Society of London A* (2020).
32 Ikari, M. J. Laboratory slow slip events in natural geological materials. *Geophysical Journal International* **218**, 354-387, doi:10.1093/gji/ggz143 (2019).
33 Ikari, M. J., Ito, Y., Ujiie, K. & Kopf, A. J. Spectrum of slip behaviour in Tohoku fault zone samples at plate tectonic slip rates. *Nature Geoscience* **8**, 870-+, doi:10.1038/ngeo2547 (2015).
34 Leeman, J. R., Marone, C. & Saffer, D. M. Frictional Mechanics of Slow Earthquakes. *J. Geophys. Res.-Solid Earth* **123**, 7931-7949, doi:10.1029/2018jb015768 (2018).
35 Reber, J. E., Lavier, L. L. & Hayman, N. W. Experimental demonstration of a semi-brittle origin for crustal strain transients. *Nature Geoscience* **8**, 712-+, doi:10.1038/ngeo2496 (2015).
36 Fagereng, A., Remitti, F. & Sibson, R. H. Incrementally developed slickenfibers - Geological record of repeating low stress-drop seismic events? *Tectonophysics* **510**, 381-386, doi:10.1016/j.tecto.2011.08.015 (2011).
37 Ujiie, K. *et al.* An Explanation of Episodic Tremor and Slow Slip Constrained by Crack-Seal Veins and Viscous Shear in Subduction Melange. *Geophys. Res. Lett.* **45**, 5371-5379, doi:10.1029/2018gl078374 (2018).
38 Behr, W. M., Kotowski, A. J. & Ashley, K. T. Dehydration-induced rheological heterogeneity and the deep tremor source in warm subduction zones. *Geology* **46**, 475-478, doi:10.1130/g40105.1 (2018).
39 Kotowski, A. J. & Behr, W. M. Length scales and types of heterogeneities along the deep subduction interface: Insights from exhumed rocks on Syros Island, Greece. *Geosphere* **15**, 1038-1065, doi:10.1130/ges02037.1 (2019).
40 Tarling, M. S., Smith, S. A. F. & Scott, J. M. Fluid overpressure from chemical reactions in serpentinite within the source region of deep episodic tremor. *Nature Geoscience* **12**, 1034-1042, doi:10.1038/s41561-019-0470-z (2019).
41 Platt, J. P., Xia, H. R. & Schmidt, W. L. Rheology and stress in subduction zones around the aseismic/seismic transition. *Progress in Earth and Planetary Science* **5**, doi:10.1186/s40645-018-0183-8 (2018).
42 Hayman, N. W. & Lavier, L. L. The geologic record of deep episodic tremor and slip. *Geology* **42**, 195-198, doi:10.1130/g34990.1 (2014).
43 Angiboust, S. *et al.* Probing the transition between seismically coupled and decoupled segments along an ancient subduction interface. *Geochemistry Geophysics Geosystems* **16**, 1905-1922, doi:10.1002/2015gc005776 (2015).
44 Saito, T., Ujiie, K., Tsutsumi, A., Kameda, J. & Shibazaki, B. Geological and frictional aspects of very-low-frequency earthquakes in an accretionary prism. *Geophys. Res. Lett.* **40**, 703-708, doi:10.1002/grl.50175 (2013).

45 Saffer, D. M. & Wallace, L. M. The frictional, hydrologic, metamorphic and thermal habitat of shallow slow earthquakes. *Nature Geoscience* **8**, 594-600, doi:10.1038/ngeo2490 (2015).
46 Audet, P. & Kim, Y. Teleseismic constraints on the geological environment of deep episodic slow earthquakes in subduction zone forearcs: A review. *Tectonophysics* **670**, 1-15, doi:10.1016/j.tecto.2016.01.005 (2016).
47 Rubinstein, J. L., Shelly, D. R. & Ellsworth, W. L. *Non-volcanic Tremor: A Window into the Roots of Fault Zones*. (2010).
48 Royer, A. A. & Bostock, M. G. A comparative study of low frequency earthquake templates in northern Cascadia. *Earth and Planetary Science Letters* **402**, 247-256, doi:10.1016/j.epsl.2013.08.040 (2014).
49 Chestler, S. R. & Creager, K. C. A Model for Low-Frequency Earthquake Slip. *Geochemistry Geophysics Geosystems* **18**, 4690-4708, doi:10.1002/2017gc007253 (2017).
50 Ide, S., Shelly, D. R. & Beroza, G. C. Mechanism of deep low frequency earthquakes: Further evidence that deep non-volcanic tremor is generated by shear slip on the plate interface. *Geophys. Res. Lett.* **34**, doi:10.1029/2006gl028890 (2007).
51 Brown, J. R. *et al.* Deep low-frequency earthquakes in tremor localize to the plate interface in multiple subduction zones. *Geophys. Res. Lett.* **36**, doi:10.1029/2009gl040027 (2009).
52 Harrington, R. M., Cochran, E. S., Griffiths, E. M., Zeng, X. F. & Thurber, C. H. Along-Strike Variations in Fault Frictional Properties along the San Andreas Fault near Cholame, California, from Joint Earthquake and Low-Frequency Earthquake Relocations. *Bulletin of the Seismological Society of America* **106**, 319-326, doi:10.1785/0120150171 (2016).
53 Walter, J. I., Schwartz, S. Y., Protti, J. M. & Gonzalez, V. Persistent tremor within the northern Costa Rica seismogenic zone. *Geophys. Res. Lett.* **38**, doi:10.1029/2010gl045586 (2011).
54 Arai, R. *et al.* Structure of the tsunamigenic plate boundary and low-frequency earthquakes in the southern Ryukyu Trench. *Nature Communications* **7**, doi:10.1038/ncomms12255 (2016).
55 Schwartz, S. Y. & Rokosky, J. M. Slow slip events and seismic tremor at circum-pacific subduction zones. *Rev. Geophys.* **45**, doi:10.1029/2006rg000208 (2007).
56 Wech, A. G., Boese, C. M., Stern, T. A. & Townend, J. Tectonic tremor and deep slow slip on the Alpine Fault. *Geophys. Res. Lett.* **39**, doi:10.1029/2012gl051751 (2012).
57 Chamberlain, C. J., Shelly, D. R., Townend, J. & Stern, T. A. Low-frequency earthquakes reveal punctuated slow slip on the deep extent of the Alpine Fault, New Zealand. *Geochemistry Geophysics Geosystems* **15**, 2984-2999, doi:10.1002/2014gc005436 (2014).
58 Hall, K., Houston, H. & Schmidt, D. Spatial Comparisons of Tremor and Slow Slip as a Constraint on Fault Strength in the Northern Cascadia Subduction Zone. *Geochemistry Geophysics Geosystems* **19**, 2706-2718, doi:10.1029/2018gc007694 (2018).
59 Brace, W. F. & Kohlstedt, D. L. LIMITS ON LITHOSPHERIC STRESS IMPOSED BY LABORATORY EXPERIMENTS. *Journal of Geophysical Research* **85**, 6248-6252, doi:10.1029/JB085iB11p06248 (1980).

60 Shelly, D. R. A 15year catalog of more than 1 million low-frequency earthquakes: Tracking tremor and slip along the deep San Andreas Fault. *J. Geophys. Res.-Solid Earth* **122**, 3739-3753, doi:10.1002/2017jb014047 (2017).
61 Shelly, D. R. Complexity of the deep San Andreas Fault zone defined by cascading tremor. *Nature Geoscience* **8**, 145-151, doi:10.1038/ngeo2335 (2015).
62 Obara, K., Tanaka, S., Maeda, T. & Matsuzawa, T. Depth-dependent activity of non-volcanic tremor in southwest Japan. *Geophys. Res. Lett.* **37**, doi:10.1029/2010gl043679 (2010).
63 Wech, A. G. Interactive Tremor Monitoring. *Seismological Research Letters* **81**, 664-669, doi:10.1785/gssrl.81.4.664 (2010).
64 Bostock, M. G., Royer, A. A., Hearn, E. H. & Peacock, S. M. Low frequency earthquakes below southern Vancouver Island. *Geochemistry Geophysics Geosystems* **13**, doi:10.1029/2012gc004391 (2012).
65 Bostock, M. G., Thomas, A. M., Savard, G., Chuang, L. & Rubin, A. M. Magnitudes and moment-duration scaling of low-frequency earthquakes beneath southern Vancouver Island. *J. Geophys. Res.-Solid Earth* **120**, 6329-6350, doi:10.1002/2015jb012195 (2015).
66 Frank, W. B. *et al.* Low-frequency earthquakes in the Mexican Sweet Spot. *Geophys. Res. Lett.* **40**, 2661-2666, doi:10.1002/grl.50561 (2013).
67 Thomas, A. M., Beroza, G. C. & Shelly, D. R. Constraints on the source parameters of low-frequency earthquakes on the San Andreas Fault. *Geophys. Res. Lett.* **43**, 1464-1471, doi:10.1002/2015gl067173 (2016).
68 Sweet, J. R., Creager, K. C. & Houston, H. A family of repeating low-frequency earthquakes at the downdip edge of tremor and slip. *Geochemistry Geophysics Geosystems* **15**, 3713-3721, doi:10.1002/2014gc005449 (2014).
69 Shelly, D. R. & Hardebeck, J. L. Precise tremor source locations and amplitude variations along the lower-crustal central San Andreas Fault. *Geophys. Res. Lett.* **37**, doi:10.1029/2010gl043672 (2010).
70 Allmann, B. P. & Shearer, P. M. Global variations of stress drop for moderate to large earthquakes. *J. Geophys. Res.-Solid Earth* **114**, doi:10.1029/2008jb005821 (2009).
71 Frank, W. B. Slow slip hidden in the noise: The intermittence of tectonic release. *Geophys. Res. Lett.* **43**, 10125-10133, doi:10.1002/2016gl069537 (2016).
72 Audet, P. & Schaeffer, A. J. Fluid pressure and shear zone development over the locked to slow slip region in Cascadia. *Science Advances* **4**, doi:10.1126/sciadv.aar2982 (2018).
73 Song, T. R. A. *et al.* Subducting Slab Ultra-Slow Velocity Layer Coincident with Silent Earthquakes in Southern Mexico. *Science* **324**, 502-506, doi:10.1126/science.1167595 (2009).
74 Shelly, D. R., Beroza, G. C., Ide, S. & Nakamula, S. Low-frequency earthquakes in Shikoku, Japan, and their relationship to episodic tremor and slip. *Nature* **442**, 188-191, doi:10.1038/nature04931 (2006).
75 Kodaira, S. *et al.* High pore fluid pressure may cause silent slip in the Nankai Trough. *Science* **304**, 1295-1298, doi:10.1126/science.1096535 (2004).
76 Audet, P., Bostock, M. G., Christensen, N. I. & Peacock, S. M. Seismic evidence for overpressured subducted oceanic crust and megathrust fault sealing. *Nature* **457**, 76-78, doi:10.1038/nature07650 (2009).
77 Rubinstein, J. L. *et al.* Non-volcanic tremor driven by large transient shear stresses. *Nature* **448**, 579-582, doi:10.1038/nature06017 (2007).

78 Thomas, A. M., Burgmann, R., Shelly, D. R., Beeler, N. M. & Rudolph, M. L. Tidal triggering of low frequency earthquakes near Parkfield, California: Implications for fault mechanics within the brittle-ductile transition. *J. Geophys. Res.-Solid Earth* **117**, doi:10.1029/2011jb009036 (2012).
79 Thomas, A. M., Nadeau, R. M. & Burgmann, R. Tremor-tide correlations and near-lithostatic pore pressure on the deep San Andreas fault. *Nature* **462**, 1048-U1105, doi:10.1038/nature08654 (2009).
80 van der Elst, N. J., Delorey, A. A., Shelly, D. R. & Johnson, P. A. Fortnightly modulation of San Andreas tremor and low-frequency earthquakes. *Proceedings of the National Academy of Sciences of the United States of America* **113**, 8601-8605, doi:10.1073/pnas.1524316113 (2016).
81 Ghosh, A. *et al.* Tremor bands sweep Cascadia. *Geophys. Res. Lett.* **37**, doi:10.1029/2009gl042301 (2010).
82 Houston, H., Delbridge, B. G., Wech, A. G. & Creager, K. C. Rapid tremor reversals in Cascadia generated by a weakened plate interface. *Nature Geoscience* **4**, 404-409, doi:10.1038/ngeo1157 (2011).
83 Moore, J. C., Rowe, C. D. & Meneghini, F. in *Seismogenic Zone of Subduction Thrust Faults* Vol. Margins: Theoretical and Experimental Earth Science Series, 2 (eds T. H. Dixon & J. C. Moore) 288-314 (Columbia University Press, 2007).
84 Moore, J. C. & Byrne, T. THICKENING OF FAULT ZONES - A MECHANISM OF MELANGE FORMATION IN ACCRETING SEDIMENTS. *Geology* **15**, 1040-1043, doi:10.1130/0091-7613(1987)15<1040:tofzam>2.0.co;2 (1987).
85 Rowe, C. D., Moore, J. C., Remitti, F. & Scientist, I. E. T. The thickness of subduction plate boundary faults from the seafloor into the seismogenic zone. *Geology* **41**, 991-994, doi:10.1130/g34556.1 (2013).
86 Stenvall, C. A., Fagereng, A. & Diener, J. F. A. Weaker Than Weakest: On the Strength of Shear Zones. *Geophys. Res. Lett.* **46**, 7404-7413, doi:10.1029/2019gl083388 (2019).
87 Lister, G. S. & Snoke, A. W. S-C MYLONITES. *J. Struct. Geol.* **6**, 617-638, doi:10.1016/0191-8141(84)90001-4 (1984).
88 Goodwin, L. B. & Tikoff, B. Competency contrast, kinematics, and the development of foliations and lineations in the crust. *J. Struct. Geol.* **24**, 1065-1085, doi:10.1016/s0191-8141(01)00092-x (2002).
89 Ujiie, K., Yamaguchi, H., Sakaguchi, A. & Toh, S. Pseudotachylytes in an ancient accretionary complex and implications for melt lubrication during subduction zone earthquakes. *J. Struct. Geol.* **29**, 599-613 (2007).
90 Cerchiari, A. *et al.* Cyclical variations of fluid sources and stress state in a shallow megathrust-zone melange. *J. Geol. Soc.* **177**, 647-659, doi:10.1144/jgs2019-072 (2020).
91 Kimura, G. *et al.* Hanging wall deformation of a seismogenic megasplay fault in an accretionary prism: The Nobeoka Thrust in southwestern Japan. *J. Struct. Geol.* **52**, 136-147, doi:10.1016/j.jsg.2013.03.015 (2013).
92 Kimura, G. *et al.* Tectonic melange as fault rock of subduction plate boundary. *Tectonophysics* **568**, 25-38, doi:10.1016/j.tecto.2011.08.025 (2012).
93 Rennie, S. F., Fagereng, A. & Diener, J. F. A. Strain distribution within a km-scale, mid-crustal shear zone: The Kuckaus Mylonite Zone, Namibia. *J. Struct. Geol.* **56**, 57-69, doi:10.1016/j.jsg.2013.09.001 (2013).

94 Fusseis, F., Handy, M. R. & Schrank, C. Networking of shear zones at the brittle-to-viscous transition (Cap de Creus, NE Spain). *J. Struct. Geol.* **28**, 1228-1243, doi:10.1016/j.jsg.2006.03.022 (2006).
95 Auzende, A. L. *et al.* Deformation mechanisms of antigorite serpentinite at subduction zone conditions determined from experimentally and naturally deformed rocks. *Earth and Planetary Science Letters* **411**, 229-240, doi:10.1016/j.epsl.2014.11.053 (2015).
96 Boutonnet, E., Leloup, P. H., Sassier, C., Gardien, V. & Ricard, Y. Ductile strain rate measurements document long-term strain localization in the continental crust. *Geology* **41**, 819-822, doi:10.1130/g33723.1 (2013).
97 Campbel, L. R. & Menegon, L. Transient High Strain Rate During Localized Viscous Creep in the Dry Lower Continental Crust (Lofoten, Norway). *J. Geophys. Res.-Solid Earth* **124**, 10240-10260, doi:10.1029/2019jb018052 (2019).
98 Skarbek, R. M., Rempel, A. W. & Schmidt, D. A. Geologic heterogeneity can produce aseismic slip transients. *Geophys. Res. Lett.* **39**, doi:10.1029/2012gl053762 (2012).
99 Moore, J. C. & Allwardt, A. PROGRESSIVE DEFORMATION OF A TERTIARY TRENCH SLOPE, KODIAK ISLANDS, ALASKA. *Journal of Geophysical Research* **85**, 4741-&, doi:10.1029/JB085iB09p04741 (1980).
100 Remitti, F., Bettelli, G. & Vannucchi, P. Internal structure and tectonic evolution of an underthrust tectonic melange: the Sestola-Vidiciatico tectonic unit of the Northern Apennines, Italy. *Geodinamica Acta* **20**, 37-51, doi:10.3166/ga.20.37-51 (2007).
101 Vannucchi, P. & Bettelli, G. Mechanisms of subduction accretion as implied from the broken formations in the Apennines, Italy. *Geology* **30**, 835-838, doi:10.1130/0091-7613(2002)030<0835:mosaai>2.0.co;2 (2002).
102 Kimura, G. & Mukai, A. UNDERPLATED UNITS IN AN ACCRETIONARY COMPLEX - MELANGE OF THE SHIMANTO BELT OF EASTERN SHIKOKU, SOUTHWEST JAPAN. *Tectonics* **10**, 31-50, doi:10.1029/90tc00799 (1991).
103 Festa, A., Ogata, K. & Pini, G. A. Polygenetic melanges: a glimpse on tectonic, sedimentary and diapiric recycling in convergent margins. *J. Geol. Soc.* **177**, 551-561, doi:10.1144/jgs2019-212 (2020).
104 Schmidt, W. L. & Platt, J. P. Subduction, accretion, and exhumation of coherent Franciscan blueschist-facies rocks, northern Coast Ranges, California. *Lithosphere* **10**, 301-326, doi:10.1130/l697.1 (2018).
105 Laurent, V. *et al.* Strain localization in a fossilized subduction channel: Insights from the Cycladic Blueschist Unit (Syros, Greece). *Tectonophysics* **672**, 150-169, doi:10.1016/j.tecto.2016.01.036 (2016).
106 Hermann, J., Muntener, O. & Scambelluri, M. The importance of serpentinite mylonites for subduction and exhumation of oceanic crust. *Tectonophysics* **327**, 225-238, doi:10.1016/s0040-1951(00)00171-2 (2000).
107 Guillot, S., Schwartz, S., Reynard, B., Agard, P. & Prigent, C. Tectonic significance of serpentinites. *Tectonophysics* **646**, 1-19, doi:10.1016/j.tecto.2015.01.020 (2015).
108 Melosh, B. L., Rowe, C. D., Gerbi, C., Smit, L. & Macey, P. Seismic cycle feedbacks in a mid-crustal shear zone. *J. Struct. Geol.* **112**, 95-111, doi:10.1016/j.jsg.2018.04.004 (2018).
109 Price, N. A. *et al.* Recrystallization fabrics of sheared quartz veins with a strong pre-existing crystallographic preferred orientation from a seismogenic shear zone. *Tectonophysics* **682**, 214-236, doi:10.1016/j.tecto.2016.05.030 (2016).

110 Fagereng, A. Frequency-size distribution of competent lenses in a block-in-matrix melange: Imposed length scales of brittle deformation? *J. Geophys. Res.-Solid Earth* **116**, doi:10.1029/2010jb007775 (2011).
111 Kitamura, Y. & Kimura, G. Dynamic role of tectonic melange during interseismic process of plate boundary mega earthquakes. *Tectonophysics* **568**, 39-52, doi:10.1016/j.tecto.2011.07.008 (2012).
112 Clauset, A., Shalizi, C. R. & Newman, M. E. J. Power-Law Distributions in Empirical Data. *Siam Review* **51**, 661-703, doi:10.1137/070710111 (2009).
113 Kitamura, Y. *et al.* Melange and its seismogenic roof decollement: A plate boundary fault rock in the subduction zone - An example from the Shimanto Belt, Japan. *Tectonics* **24**, doi:10.1029/2004tc001635 (2005).
114 Fagereng, A. & den Hartog, S. A. M. Subduction megathrust creep governed by pressure solution and frictional-viscous flow. *Nature Geoscience* **10**, 51-57, doi:10.1038/ngeo2857 (2017).
115 Tulley, C. J., Fagereng, A. & Ujiie, K. Hydrous oceanic crust hosts megathrust creep at low shear stresses. *Science Advances* **6**, eaba1529, doi:10.1126/sciadv.aba1529 (2020).
116 Melosh, B. L. *et al.* Snap, Crackle, Pop: Dilational fault breccias record seismic slip below the brittle-plastic transition. *Earth and Planetary Science Letters* **403**, 432-445, doi:10.1016/j.epsl.2014.07.002 (2014).
117 Phillips, N. J., Belzer, B., French, M. E., Rowe, C. D. & Ujiie, K. Frictional Strengths of Subduction Thrust Rocksin the Region of Shallow Slow Earthquakes. *J. Geophys. Res.-Solid Earth* **125**, e2019JB018888, doi:https://doi.org/10.1029/2019JB018888 (2020).
118 Swanson, M. T. Fault structure, wear mechanisms and rupture processes in pseudotachylyte generation. *Tectonophysics* **204**, 223-242 (1992).
119 Price, N. A., Johnson, S. E., Gerbi, C. C. & West, D. P. Identifying deformed pseudotachylyte and its influence on the strength and evolution of a crustal shear zone at the base of the seismogenic zone. *Tectonophysics* **518**, 63-83, doi:10.1016/j.tecto.2011.11.011 (2012).
120 Goodwin, L. B. & Wenk, H. R. Development Of Phyllonite From Granodiorite - Mechanisms Of Grain-Size Reduction In The Santa-Rosa Mylonite Zone, California. *J. Struct. Geol.* **17**, 689-& (1995).
121 Niemeijer, A. R. & Spiers, C. J. Influence of phyllosilicates on fault strength in the brittle-ductile transition: Insights from rock analogue experiments. *Geological Society of London Special Publications* **245**, 303-327, doi:doi:10.1144/GSL.SP.2005.245.01.15 (2005).
122 Wassmann, S. & Stockhert, B. Rheology of the plate interface - Dissolution precipitation creep in high pressure metamorphic rocks. *Tectonophysics* **608**, 1-29, doi:10.1016/j.tecto.2013.09.030 (2013).
123 Compton, K. E., Kirkpatrick, J. D. & Holk, G. J. Cyclical shear fracture and viscous flow during transitional ductile-brittle deformation in the Saddlebag Lake Shear Zone, California. *Tectonophysics* **708**, 1-14, doi:10.1016/j.tecto.2017.04.006 (2017).
124 Meneghini, F. & Moore, J. C. Deformation and hydrofracture in a subduction thrust at seismogenic depths: The Rodeo Cove thrust zone, Marin Headlands, California. *Geol. Soc. Am. Bull.* **119**, 174-183, doi:10.1130/b25807.1 (2007).
125 Fagereng, A., Hillary, G. W. B. & Diener, J. F. A. Brittle-viscous deformation, slow slip, and tremor. *Geophys. Res. Lett.* **41**, 4159-4167, doi:10.1002/2014gl060433 (2014).

126 Palazzin, G. *et al.* Deformation processes at the down-dip limit of the seismogenic zone: The example of Shimanto accretionary complex. *Tectonophysics* **687**, 28-43, doi:10.1016/j.tecto.2016.08.013 (2016).
127 Rowe, C. D. *et al.* Geometric Complexity of Earthquake Rupture Surfaces Preserved in Pseudotachylyte Networks. *J. Geophys. Res.-Solid Earth* **123**, 7998-8015, doi:10.1029/2018jb016192 (2018).
128 Melosh, B. L., Rowe, C. D., Gerbi, C., Bate, C. E. & Shulman, D. The spin zone: Transient mid-crust permeability caused by coseismic brecciation. *J. Struct. Geol.* **87**, 47-63, doi:10.1016/j.jsg.2016.04.003 (2016).
129 Gosselin, J. M. *et al.* Seismic evidence for megathrust fault-valve behavior during episodic tremor and slip. *Science Advances* **6**, doi:10.1126/sciadv.aay5174 (2020).
130 French, M. E. & Condit, C. B. Slip partitioning along an idealized subduction plate boundary at deep slow slip conditions. *Earth and Planetary Science Letters* **528**, doi:10.1016/j.epsl.2019.115828 (2019).
131 Fagereng, A., Remitti, F. & Sibson, R. H. Shear veins observed within anisotropic fabric at high angles to the maximum compressive stress. *Nature Geoscience* **3**, 482-485, doi:10.1038/ngeo898 (2010).
132 Jaeger, J. C., Cook, N. G. W. & Zimmerman, R. W. *Fundamentals of Rock Mechanics*. Fourth edn, (Blackwell Publishing, 2007).
133 Shea, W. T. & Kronenberg, A. K. STRENGTH AND ANISOTROPY OF FOLIATED ROCKS WITH VARIED MICA CONTENTS. *J. Struct. Geol.* **15**, 1097-1121, doi:10.1016/0191-8141(93)90158-7 (1993).
134 Rowe, C. D., Meneghini, F. & Moore, J. C. Fluid-rich damage zone of an ancient out-of-sequence thrust, Kodiak Islands, Alaska. *Tectonics* **28**, doi:10.1029/2007tc002126 (2009).
135 Fagereng, A., Diener, J. F. A., Meneghini, F., Harris, C. & Kvadsheim, A. Quartz vein formation by local dehydration embrittlement along the deep, tremorgenic subduction thrust interface. *Geology* **46**, 67-70, doi:10.1130/g39649.1 (2018).
136 Fabbri, O. *et al.* Deformation structures from splay and décollement faults in the Nankai accretionary prism, SW Japan (IODP NanTroSEIZE Expedition 316). Evidence for slow and rapid slip in fault rocks. *Geochemistry Geophysics Geosystems*, doi:10.1029/2019GC008786 (2020).
137 Bos, B. & Spiers, C. J. Frictional-viscous flow of phyllosilicate-bearing fault rock: Microphysical model and implications for crustal strength profiles. *J. Geophys. Res.-Solid Earth* **107** (2002).
138 Rowe, C. D., Meneghini, F. & Moore, J. C. in *Geology of the Earthquake Source: a Volume in Honour of Rick Sibson* Vol. 359 *Geological Society Special Publication* (eds A. Fagereng, V. G. Toy, & J. V. Rowland) 77-95 (2011).
139 Rutter, E. H., Maddock, R. H., Hall, S. H. & White, S. H. COMPARATIVE MICROSTRUCTURES OF NATURAL AND EXPERIMENTALLY PRODUCED CLAY-BEARING FAULT GOUGES. *Pure Appl. Geophys.* **124**, 3-30, doi:10.1007/bf00875717 (1986).
140 Kirkpatrick, J. D. *et al.* Structure and lithology of the Japan Trench subduction plate boundary fault. *Tectonics* **34**, 53-69, doi:10.1002/2014tc003695 (2015).
141 Fagereng, A. *et al.* Mixed deformation styles observed on a shallow subduction thrust, Hikurangi margin, New Zealand. *Geology* **47**, 872-876, doi:10.1130/g46367.1 (2019).

142 Beall, A., Fagereng, A. & Ellis, S. Strength of Strained Two-Phase Mixtures: Application to Rapid Creep and Stress Amplification in Subduction Zone Melange. *Geophys. Res. Lett.* **46**, 169-178, doi:10.1029/2018gl081252 (2019).
143 Sibson, R. H. Tensile overpressure compartments on low-angle thrust faults. *Earth Planets and Space* **69**, doi:10.1186/s40623-017-0699-y (2017).
144 Sibson, R. H. Structural permeability of fluid-driven fault-fracture meshes. *J. Struct. Geol.* **18**, 1031-1042, doi:10.1016/0191-8141(96)00032-6 (1996).
145 Beall, A., Fagereng, A. & Ellis, S. Fracture and Weakening of Jammed Subduction Shear Zones, Leading to the Generation of Slow Slip Events. *Geochemistry Geophysics Geosystems* **20**, 4869–4884, doi:doi.org/10.1029/2019GC008481 (2019).
146 Stunitz, H. & Tullis, J. Weakening and strain localization produced by syn-deformational reaction of plagioclase. *Int. J. Earth Sci.* **90**, 136-148, doi:10.1007/s005310000148 (2001).
147 Rubin, A. M. Designer friction laws for bimodal slow slip propagation speeds. *Geochemistry Geophysics Geosystems* **12**, doi:10.1029/2010gc003386 (2011).
148 Leeman, J. R., Saffer, D. M., Scuderi, M. M. & Marone, C. Laboratory observations of slow earthquakes and the spectrum of tectonic fault slip modes. *Nature Communications* **7**, doi:10.1038/ncomms11104 (2016).
149 Liu, Y. J. & Rice, J. R. Spontaneous and triggered aseismic deformation transients in a subduction fault model. *J. Geophys. Res.-Solid Earth* **112**, doi:10.1029/2007jb004930 (2007).
150 Hawthorne, J. C. & Rubin, A. M. Laterally propagating slow slip events in a rate and state friction model with a velocity-weakening to velocity-strengthening transition. *J. Geophys. Res.-Solid Earth* **118**, 3785-3808, doi:10.1002/jgrb.50261 (2013).
151 Shibazaki, B. & Shimamoto, T. Modelling of short-interval silent slip events in deeper subduction interfaces considering the frictional properties at the unstable-stable transition regime. *Geophysical Journal International* **171**, 191-205, doi:10.1111/j.1365-246X.2007.03434.x (2007).
152 Im, K., Saffer, D., Marone, C. & Avouac, J. P. Slip-rate-dependent friction as a universal mechanism for slow slip events. *Nature Geoscience* **13**, 705-+, doi:10.1038/s41561-020-0627-9 (2020).
153 Segall, P., Rubin, A. M., Bradley, A. M. & Rice, J. R. Dilatant strengthening as a mechanism for slow slip events. *J. Geophys. Res.-Solid Earth* **115**, doi:10.1029/2010jb007449 (2010).
154 Liu, Y. J. & Rubin, A. M. Role of fault gouge dilatancy on aseismic deformation transients. *J. Geophys. Res.-Solid Earth* **115**, doi:10.1029/2010jb007522 (2010).
155 Romanet, P., Bhat, H. S., Jolivet, R. & Madariaga, R. Fast and Slow Slip Events Emerge Due to Fault Geometrical Complexity. *Geophys. Res. Lett.* **45**, 4809-4819, doi:10.1029/2018gl077579 (2018).
156 Ikari, M. J. & Saffer, D. M. Comparison of frictional strength and velocity dependence between fault zones in the Nankai accretionary complex. *Geochemistry Geophysics Geosystems* **12**, doi:10.1029/2010gc003442 (2011).
157 Roesner, A. *et al.* Friction experiments under in-situ stress reveal unexpected velocity-weakening in Nankai accretionary prism samples. *Earth and Planetary Science Letters* **538**, doi:10.1016/j.epsl.2020.116180 (2020).

158 Kaproth, B. M. & Marone, C. Slow Earthquakes, Preseismic Velocity Changes, and the Origin of Slow Frictional Stick-Slip. *Science* **341**, 1229-1232, doi:10.1126/science.1239577 (2013).
159 Phillips, N. J., Motohashi, G., Ujiie, K. & Rowe, C. D. Evidence of Localized Failure Along Altered Basaltic Blocks in Tectonic Mélange at the Updip Limit of the Seismogenic Zone: Implications for the Shallow Slow Earthquake Source. *Geochemistry, Geophysics, Geosystems*, doi:https://doi.org/10.1029/2019GC008839 (2020).
160 van den Ende, M. P. A. & Niemeijer, A. R. Time-Dependent Compaction as a Mechanism for Regular Stick-Slips. *Geophys. Res. Lett.* **45**, 5959-5967, doi:10.1029/2018gl078103 (2018).
161 Hobbs, B. E., Ord, A. & Teyssier, C. EARTHQUAKES IN THE DUCTILE REGIME. *Pure Appl. Geophys.* **124**, 309-336, doi:10.1007/bf00875730 (1986).
162 Sibson, R. H. Transient Discontinuities In Ductile Shear Zones. *J. Struct. Geol.* **2**, 165-& (1980).
163 French, M. E., Hirth, G. & Okazaki, K. Fracture-induced pore fluid pressure weakening and dehydration of serpentinite. *Tectonophysics* **767**, 11, doi:10.1016/j.tecto.2019.228168 (2019).
164 Kato, A., Sakaguchi, A., Yoshida, S., Yamaguchi, H. & Kaneda, Y. Permeability structure around an ancient exhumed subduction-zone fault. *Geophys. Res. Lett.* **31**, doi:10.1029/2003gl019183 (2004).
165 Kawano, S., Katayama, I. & Okazaki, K. Permeability anisotropy of serpentinite and fluid pathways in a subduction zone. *Geology* **39**, 939-942, doi:10.1130/g32173.1 (2011).
166 Okazaki, K., Katayama, I. & Noda, H. Shear-induced permeability anisotropy of simulated serpentinite gouge produced by triaxial deformation experiments. *Geophys. Res. Lett.* **40**, doi:10.1002/grl.50302 (2013).
167 Daigle, H. & Screaton, E. J. Evolution of sediment permeability during burial and subduction. *Geofluids* **15**, 84-105, doi:10.1111/gfl.12090 (2015).
168 Okazaki, K. & Katayama, I. Slow stick slip of antigorite serpentinite under hydrothermal conditions as a possible mechanism for slow earthquakes. *Geophys. Res. Lett.* **42**, 1099-1104, doi:10.1002/2014gl062735 (2015).
169 White, J. C. Paradoxical pseudotachylyte - Fault melt outside the seismogenic zone. *J. Struct. Geol.* **38**, 11-20, doi:10.1016/j.jsg.2011.11.016 (2012).
170 Chestler, S. R. & Creager, K. C. Evidence for a scale-limited low-frequency earthquake source process. *J. Geophys. Res.-Solid Earth* **122**, 3099-3114, doi:10.1002/2016jb013717 (2017).
171 Nakano, M., Yabe, S., Sugioka, H., Shinohara, M. & Ide, S. Event Size Distribution of Shallow Tectonic Tremor in the Nankai Trough. *Geophys. Res. Lett.* **46**, 5828-5836, doi:10.1029/2019gl083029 (2019).
172 Peacock, S. M. Thermal and metamorphic environment of subduction zone episodic tremor and slip. *J. Geophys. Res.-Solid Earth* **114**, doi:10.1029/2008jb005978 (2009).
173 Rubin, A. M. Episodic slow slip events and rate-and-state friction. *J. Geophys. Res.-Solid Earth* **113**, doi:10.1029/2008jb005642 (2008).
174 Daub, E. G., Shelly, D. R., Guyer, R. A. & Johnson, P. A. Brittle and ductile friction and the physics of tectonic tremor. *Geophys. Res. Lett.* **38**, doi:10.1029/2011gl046866 (2011).

175 Hawthorne, J. C., Thomas, A. M. & Ampuero, J. P. The rupture extent of low frequency earthquakes near Parkfield, CA. *Geophysical Journal International* **216**, 621-639, doi:10.1093/gji/ggy429 (2019).
176 Bostock, M. G., Thomas, A. M., Rubin, A. M. & Christensen, N. I. On corner frequencies, attenuation, and low-frequency earthquakes. *J. Geophys. Res.-Solid Earth* **122**, 543-557, doi:10.1002/2016jb013405 (2017).
177 Nowack, R. L. & Bostock, M. G. Scattered waves from low-frequency earthquakes and plate boundary structure in northern Cascadia. *Geophys. Res. Lett.* **40**, 4238-4243, doi:10.1002/grl.50826 (2013).
178 Ghosh, A. *et al.* Rapid, continuous streaking of tremor in Cascadia. *Geochemistry Geophysics Geosystems* **11**, doi:10.1029/2010gc003305 (2010).
179 Audet, P. & Burgmann, R. Possible control of subduction zone slow-earthquake periodicity by silica enrichment. *Nature* **510**, 389-+, doi:10.1038/nature13391 (2014).
180 Houston, H. Low friction and fault weakening revealed by rising sensitivity of tremor to tidal stress. *Nature Geoscience* **8**, 409-+, doi:10.1038/ngeo2419 (2015).
181 Sweet, J. R., Creager, K. C., Houston, H. & Chestler, S. R. Variations in Cascadia Low-Frequency Earthquake Behavior With Downdip Distance. *Geochemistry Geophysics Geosystems* **20**, 1202-1217, doi:10.1029/2018gc007998 (2019).
182 Hall, K., Schmidt, D. & Houston, H. Peak Tremor Rates Lead Peak Slip Rates During Propagation of Two Large Slow Earthquakes in Cascadia. *Geochemistry Geophysics Geosystems* **20**, 4665-4675, doi:10.1029/2019gc008510 (2019).
183 Obara, K., Hirose, H., Yamamizu, F. & Kasahara, K. Episodic slow slip events accompanied by non-volcanic tremors in southwest Japan subduction zone. *Geophys. Res. Lett.* **31**, doi:10.1029/2004gl020848 (2004).
184 Shelly, D. R., Beroza, G. C. & Ide, S. Complex evolution of transient slip derived from precise tremor locations in western Shikoku, Japan. *Geochemistry Geophysics Geosystems* **8**, doi:10.1029/2007gc001640 (2007).
185 Rubinstein, J. L., La Rocca, M., Vidale, J. E., Creager, K. C. & Wech, A. G. Tidal modulation of nonvolcanic tremor. *Science* **319**, 186-189, doi:10.1126/science.1150558 (2008).
186 Bostock, M. G. & Christensen, N. I. Split from slip and schist: Crustal anisotropy beneath northern Cascadia from non-volcanic tremor. *J. Geophys. Res.-Solid Earth* **117**, doi:10.1029/2011jb009095 (2012).
187 Zal, H. J. *et al.* Temporal and spatial variations in seismic anisotropy and VP/VS ratios in a region of slow slip. *Earth and Planetary Science Letters* **532**, 115970, doi:https://doi.org/10.1016/j.epsl.2019.115970 (2020).
188 Peacock, S. M. & Wang, K. Seismic consequences of warm versus cool subduction metamorphism: Examples from southwest and northeast Japan. *Science* **286**, 937-939, doi:10.1126/science.286.5441.937 (1999).
189 Matsuzawa, T., Asano, Y. & Obara, K. Very low frequency earthquakes off the Pacific coast of Tohoku, Japan. *Geophys. Res. Lett.* **42**, 4318-4325, doi:10.1002/2015gl063959 (2015).
190 Baba, S., Takeo, A., Obara, K., Matsuzawa, T. & Maeda, T. Comprehensive Detection of Very Low Frequency Earthquakes Off the Hokkaido and Tohoku Pacific Coasts, Northeastern Japan. *J. Geophys. Res.-Solid Earth* **125**, 13, doi:10.1029/2019jb017988 (2020).

191 Ito, Y. *et al.* Episodic slow slip events in the Japan subduction zone before the 2011 Tohoku-Oki earthquake. *Tectonophysics* **600**, 14-26, doi:10.1016/j.tecto.2012.08.022 (2013).
192 Yamashita, Y. *et al.* Migrating tremor off southern Kyushu as evidence for slow slip of a shallow subduction interface. *Science* **348**, 676-679 (2015).
193 Sugioka, H. *et al.* Tsunamigenic potential of the shallow subduction plate boundary inferred from slow seismic slip. *Nature Geoscience* **5**, 414-418, doi:10.1038/ngeo1466 (2012).
194 Nakano, M., Hori, T., Araki, E., Kodaira, S. & Ide, S. Shallow very-low-frequency earthquakes accompany slow slip events in the Nankai subduction zone. *Nature Communications* **9**, doi:10.1038/s41467-018-03431-5 (2018).
195 Annoura, S., Obara, K. & Maeda, T. Total energy of deep low-frequency tremor in the Nankai subduction zone, southwest Japan. *Geophys. Res. Lett.* **43**, 2562-2567, doi:10.1002/2016gl067780 (2016).
196 Peacock, S. M. *et al.* Thermal structure of the Costa Rica - Nicaragua subduction zone. *Phys. Earth Planet. Inter.* **149**, 187-200, doi:10.1016/j.pepi.2004.08.030 (2005).
197 Walter, J. I., Schwartz, S. Y., Protti, M. & Gonzalez, V. The synchronous occurrence of shallow tremor and very low frequency earthquakes offshore of the Nicoya Peninsula, Costa Rica. *Geophys. Res. Lett.* **40**, 1517-1522, doi:10.1002/grl.50213 (2013).
198 Gutscher, M. A. & Peacock, S. M. Thermal models of flat subduction and the rupture zone of great subduction earthquakes. *J. Geophys. Res.-Solid Earth* **108**, doi:10.1029/2001jb000787 (2003).
199 Nakamura, M. & Sunagawa, N. Activation of very low frequency earthquakes by slow slip events in the Ryukyu Trench. *Geophys. Res. Lett.* **42**, 1076-1082, doi:10.1002/2014gl062929 (2015).
200 Nakamura, M. Distribution of low-frequency earthquakes accompanying the very low frequency earthquakes along the Ryukyu Trench. *Earth Planets and Space* **69**, doi:10.1186/s40623-017-0632-4 (2017).
201 Ando, M., Tu, Y., Kumagai, H., Yamanaka, Y. & Lin, C. H. Very low frequency earthquakes along the Ryukyu subduction zone. *Geophys. Res. Lett.* **39**, doi:10.1029/2011gl050559 (2012).
202 Fagereng, A. & Ellis, S. On factors controlling the depth of interseismic coupling on the Hikurangi subduction interface, New Zealand. *Earth and Planetary Science Letters* **278**, 120-130, doi:10.1016/j.epsl.2008.11.033 (2009).
203 Todd, E. K. & Schwartz, S. Y. Tectonic tremor along the northern Hikurangi Margin, New Zealand, between 2010 and 2015. *J. Geophys. Res.-Solid Earth* **121**, 8706-8719, doi:10.1002/2016jb013480 (2016).
204 Currie, C. A., Hyndman, R. D., Wang, K. & Kostoglodov, V. Thermal models of the Mexico subduction zone: Implications for the megathrust seismogenic zone. *J. Geophys. Res.-Solid Earth* **107**, doi:10.1029/2001jb000886 (2002).
205 Frank, W. B. *et al.* Using systematically characterized low-frequency earthquakes as a fault probe in Guerrero, Mexico. *J. Geophys. Res.-Solid Earth* **119**, 7686-7700, doi:10.1002/2014jb011457 (2014).
206 Husker, A. L. *et al.* Temporal variations of non-volcanic tremor (NVT) locations in the Mexican subduction zone: Finding the NVT sweet spot. *Geochemistry Geophysics Geosystems* **13**, doi:10.1029/2011gc003916 (2012).

207 Wech, A. G. & Bartlow, N. M. Slip rate and tremor genesis in Cascadia. *Geophys. Res. Lett.* **41**, 392-398, doi:10.1002/2013gl058607 (2014).
208 Bostock, M. G., Christensen, N. I. & Peacock, S. M. Seismicity in Cascadia. *Lithos* **332**, 55-66, doi:10.1016/j.lithos.2019.02.019 (2019).
209 Shi, Y. L., Allis, R. & Davey, F. Thermal modeling of the Southern Alps, New Zealand. *Pure Appl. Geophys.* **146**, 469-501, doi:10.1007/bf00874730 (1996).
210 Wech, A. G. *et al.* Tectonic Tremor Recorded by Ocean Bottom Seismometers. *Seismological Research Letters* **84**, 752-758, doi:10.1785/0220120184 (2013).
211 Yamato, P., Mouthereau, F. & Burov, E. Taiwan mountain building: insights from 2-D thermomechanical modelling of a rheologically stratified lithosphere. *Geophysical Journal International* **176**, 307-326, doi:10.1111/j.1365-246X.2008.03977.x (2009).
212 Aguiar, A. C., Chao, K. & Beroza, G. C. Tectonic tremor and LFEs on a reverse fault in Taiwan. *Geophys. Res. Lett.* **44**, 6683-6691, doi:10.1002/2016gl072148 (2017).
213 Chuang, L. Y., Chen, K. H., Wech, A., Byrne, T. & Peng, W. Ambient tremors in a collisional orogenic belt. *Geophys. Res. Lett.* **41**, 1485-1491, doi:10.1002/2014gl059476 (2014).
214 Tang, C. C., Peng, Z., Chao, K., Chen, C. H. & Lin, C. H. Detecting low-frequency earthquakes within non-volcanic tremor in southern Taiwan triggered by the 2005 Mw8.6 Nias earthquake. *Geophys. Res. Lett.* **37**, doi:10.1029/2010gl043918 (2010).
215 Sass, J. H. *et al.* THERMAL REGIME OF THE SOUTHERN BASIN AND RANGE PROVINCE .1. HEAT-FLOW DATA FROM ARIZONA AND THE MOJAVE DESERT OF CALIFORNIA AND NEVADA. *J. Geophys. Res.-Solid Earth* **99**, 22093-22119, doi:10.1029/94jb01891 (1994).
216 Chao, K., Peng, Z. G., Fabian, A. & Ojha, L. Comparisons of Triggered Tremor in California. *Bulletin of the Seismological Society of America* **102**, 900-908, doi:10.1785/0120110151 (2012).
217 Fagereng, A. & Diener, J. F. A. San Andreas Fault tremor and retrograde metamorphism. *Geophys. Res. Lett.* **38**, doi:10.1029/2011gl049550 (2011).
218 Marcaillou, B. *et al.* Seismogenic zone temperatures and heat-flow anomalies in the To-nankai margin segment based on temperature data from IODP expedition 333 and thermal model. *Earth and Planetary Science Letters* **349**, 171-185, doi:10.1016/j.epsl.2012.06.048 (2012).

Figures

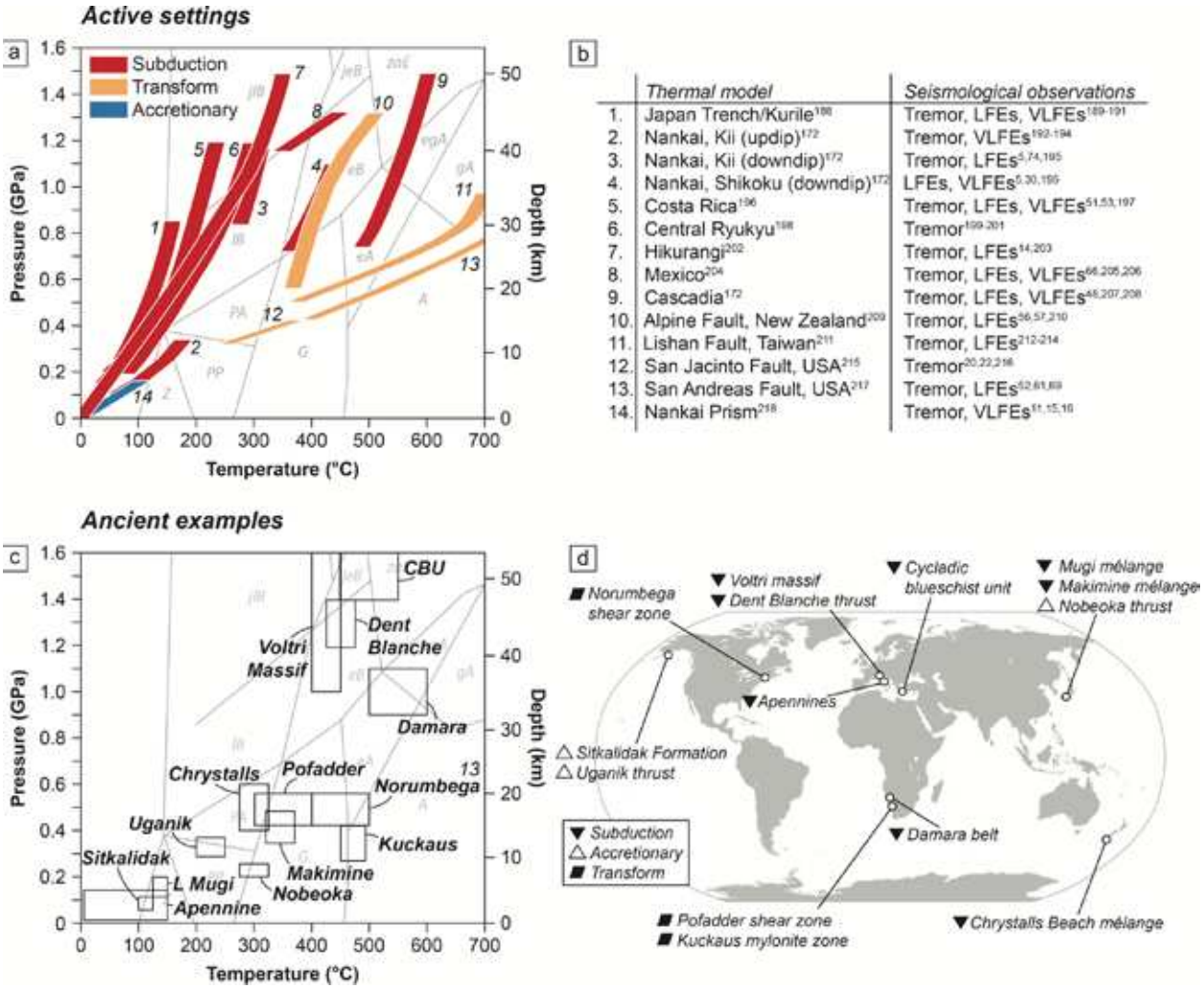

	Thermal model	Seismological observations
1.	Japan Trench/Kurile[188]	Tremor, LFEs, VLFEs[189-191]
2.	Nankai, Kii (updip)[172]	Tremor, VLFEs[192-194]
3.	Nankai, Kii (downdip)[172]	Tremor, LFEs[5,74,195]
4.	Nankai, Shikoku (downdip)[172]	LFEs, VLFEs[5,30,155]
5.	Costa Rica[196]	Tremor, LFEs, VLFEs[51,53,197]
6.	Central Ryukyu[198]	Tremor[199-201]
7.	Hikurangi[202]	Tremor, LFEs[14,203]
8.	Mexico[204]	Tremor, LFEs, VLFEs[66,205,206]
9.	Cascadia[172]	Tremor, LFEs, VLFEs[45,207,208]
10.	Alpine Fault, New Zealand[209]	Tremor, LFEs[56,57,210]
11.	Lishan Fault, Taiwan[211]	Tremor, LFEs[212-214]
12.	San Jacinto Fault, USA[215]	Tremor[20,22,216]
13.	San Andreas Fault, USA[217]	Tremor, LFEs[62,81,89]
14.	Nankai Prism[218]	Tremor, VLFEs[11,15,16]

Figure 1. Metamorphic conditions of representative seismologically observed slow earthquakes and ancient, exhumed structures selected for comparison. Depths of low frequency earthquakes and tremor highlight the wide range of tectonic and metamorphic settings that exhibit the spectrum of slow slip. a. Approximate pressure and temperature range at the source of slow earthquakes based on published thermal models and hypocentral depth distributions/relocations of seismologically observed slow earthquakes in some representative tectonic settings. Conditions for Costa Rica, Central Ryukyu, and Hikurangi subduction zones are based on epicentral locations and assume slow earthquakes occur on the plate interface. Hypocentral depths are converted to pressure assuming a linear lithostatic load and rock density of 2750 kg/m^3 for depth ≤ 30 km and 3300 kg/m^3 for depth > 30 km for comparison. Metamorphic facies for basaltic rocks shown for reference[172] (A, amphibolite; eA, epidote amphibolite; eB, epidote blueschist; egA, epidote-garnet amphibolite; G, greenschist; gA, garnet-amphibolite; jeB, jadeite-epidote

1361 blueschist; jlB, jadeite-lawsonite blueschist; lB, lawsonite blueschist; PA, prehnite-actinolite; PP, prehnite-
1362 pumpellyite; Z, zeolite; zaE, zoisite amphibole eclogite facies). b. Sources of thermal models and slow earthquake
1363 locations used to construct part a. c. Pressure and temperature conditions of deformation of ancient examples
1364 selected as representative of the range of conditions of slow earthquakes shown in a. Abbreviations in grey as in a. c.
1365 Locations of exhumed deformation structures used in this review as potential hosts of ancient slow earthquakes.
1366

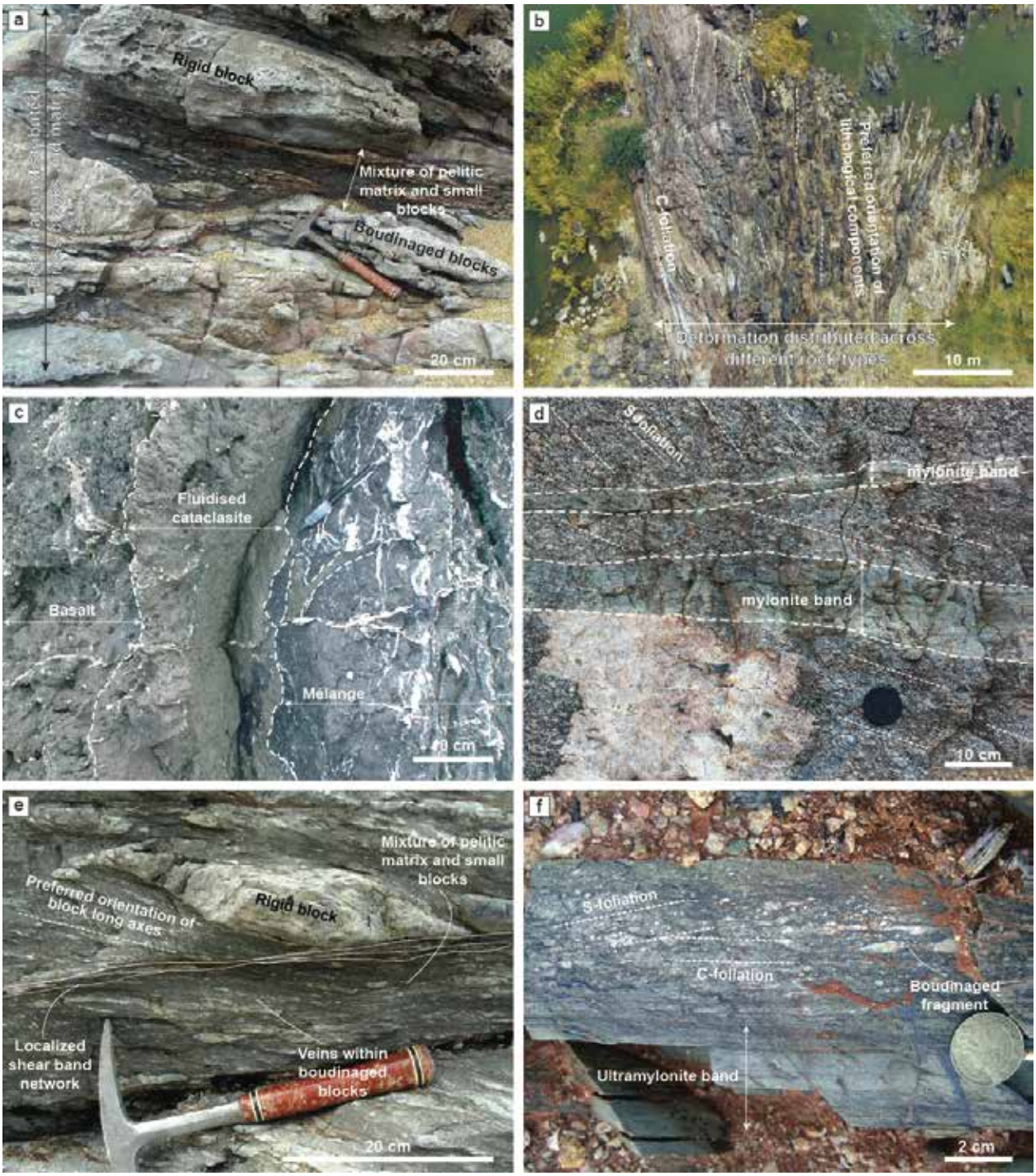

Figure 2. Photographs illustrating different types of structures associated with high strain zones. High strain zones in all tectonic settings exhibit structures with a range of thicknesses. a. Photograph of the Chrystalls Beach accretionary mélange, New Zealand, showing deformation distributed over several meters within the high strain zone. Boudinage of light grey blocks of sandstone shows they were relatively rigid during deformation. b.

Ultracataclasite layer from a seismogenic thrust fault that developed at the margin of the Mugi mélange, Japan. Injection veins contain fluidized gouge that was deformed at seismic slip rates. c. Detail of a localized shear band network within the Chrystalls Beach mélange cutting the matrix between competent blocks. Note the matrix in a. is a mixture of phyllosilicate-rich pelitic rock and small blocks of sandstone. Blocks of all sizes locally have parallel long axes. d. Aerial photo of the Pofadder shear zone, Namibia, showing deformation distributed over tens of meters. Variations in colour within the high strain zone correspond to mylonites and ultramylonites developed from different lithologies. e. Approximately 10-20 cm-thick mylonite bands developed within the Pofadder Shear Zone, Namibia. f. Example of a foliated mylonite and localized (~cm-thick) ultramylonite band from the Kuckaus mylonite zone, Namibia. The mylonite contains mm-thick shear bands that define a S-C composite fabric.

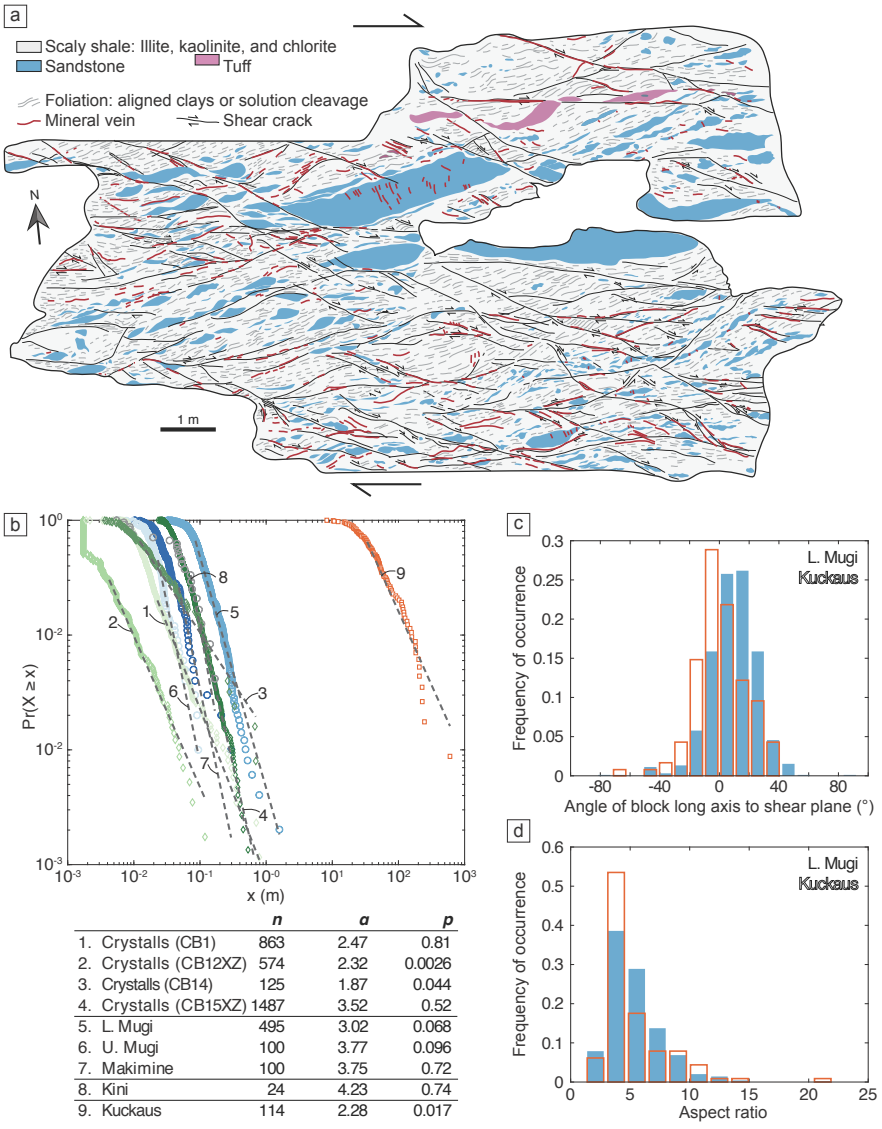

		n	*α*	*p*
1.	Crystalls (CB1)	863	2.47	0.81
2.	Crystalls (CB12XZ)	574	2.32	0.0026
3.	Crystalls (CB14)	125	1.87	0.044
4.	Crystalls (CB15XZ)	1487	3.52	0.52
5.	L. Mugi	495	3.02	0.068
6.	U. Mugi	100	3.77	0.096
7.	Makimine	100	3.75	0.72
8.	Kini	24	4.23	0.74
9.	Kuckaus	114	2.28	0.017

Figure 3. Comparison of block populations from different tectonic settings, which show similar characteristics a. Outcrop map of an exposure of the Mugi mélange showing the distribution of blocks in a pelitic matrix (scaly shale), locations of shear bands and veins, and attitudes of solution cleavages (adapted with permission from REF[92]). b. Histogram showing distribution of angle between block long axes and the shear plane orientation for the Mugi mélange (shown in a.) and the Kuckaus mylonite zone[93], a continental transform. c. Probability density functions of block long axis distributions for various high strain zones. Data from: Chrystalls Beach[110]; Upper Mugi[111]; Lower Mugi[92]; Makimine[111]; Kini[39]; Kuckaus[93] high strain zones. Dashed lines show range over which a power law was fit. Table legend beneath shows *n*, number of blocks in each dataset, α, power-law scaling exponent fitted using maximum likelihood fitting methods[112], and *p*, the result of a goodness of fit test to establish whether a

power law is a plausible fit to the data (following REF[112], power law is ruled out if $p \leq 0.1$, though p is only reliable for datasets with $n >> 100$). d. Histogram of block aspect ratios in the Mugi mélange (shown in a.) and the Kuckaus mylonite zone.

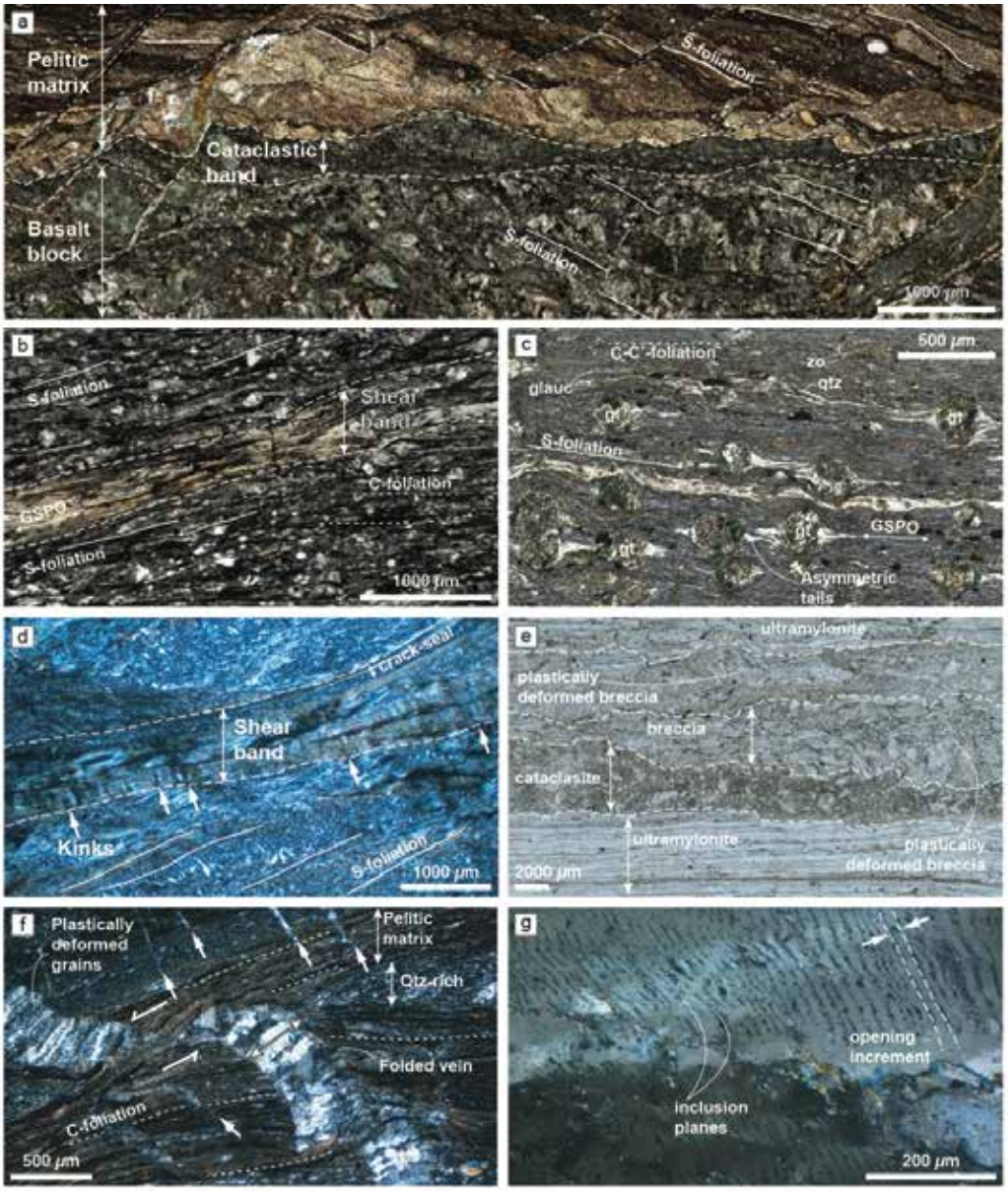

Figure 4. Examples of micro-scale structures in ancient equivalents of active slow earthquake source regions. These images show the variety of deformation mechanisms that accommodate strain across the wide range of tectonic and metamorphic environments of slow earthquakes. a. Cataclastic band developed along the margin of a basaltic block from the Mugi mélange, Japan, courtesy of Noah Phillips. b. Shear band cutting the pelitic matrix of the Makimine mélange, Japan. Phyllosilicates within the shear band exhibit a grain shape preferred orientation (GSPO) parallel to shear band margins. Pelitic matrix contains a composite S-C fabric. S-foliation resulted from dissolution-precipitation creep in quartz. c. Mafic mylonite that developed at blueschist-eclogite conditions in the

Cycladic Blueschist Unit, Greece. Grain shape preferred orientation (GSPO) in glaucophane (glauc) defines a C-C' foliation, the tails of quartz (qtz) are aligned with the S-foliation (image courtesy of Alissa Kotowski. Other mineral abbreviations are: gt = garnet; zo = zoisite). d. Antigorite mylonite from the Mie mélange, Japan in which a shear band contains antigorite with grain shape preferred orientation. Antigorite grains contain kink bands (kinks) at high angle to shear band margin. e. Strands of cataclasite and breccia developed parallel to mylonitic foliation, some of which were subsequently plastically deformed, Pofadder Shear Zone, Namibia (image courtesy of Christie Rowe). f. Extensional quartz vein that formed discordant to foliation in the Makimine mélange (white arrow with black outline shows opening vector), which was subsequently offset by shear along the C-foliation and plastically deformed. Note thinner quartz veins at high angle to C-foliation are not folded, indicating cyclical fracture and plastic deformation. g. Fluid inclusion trails (indicated by dashed white lines), which represent increments of extensional opening within a quartz vein from the Makimine mélange, Japan. The thickness of quartz between the white arrows is the interpreted opening amount in one increment.

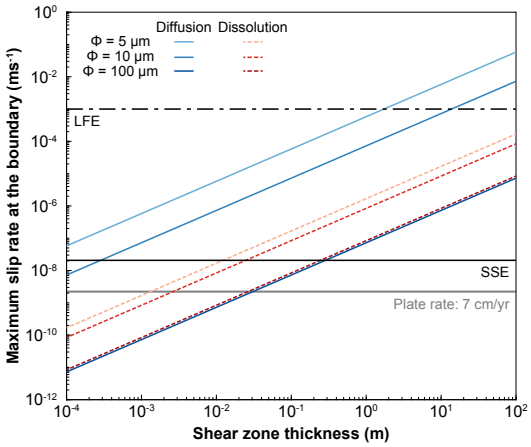

Figure 5. Upper bounds on the slip rate at a shear zone boundary that can be accommodated by dissolution-precipitation creep in the matrix of the Mugi mélange given a range of possible shear zone thicknesses. Calculations were performed assuming the shear stress driving dissolution-precipitation creep was limited by the shear stress to initiate frictional sliding (i.e. the effective shear stress was limited to 1 MPa as suggested by field observations[37,131]), for the range of grain sizes (Φ) shown, temperature of 135 °C and grain aspect ratio of 3.

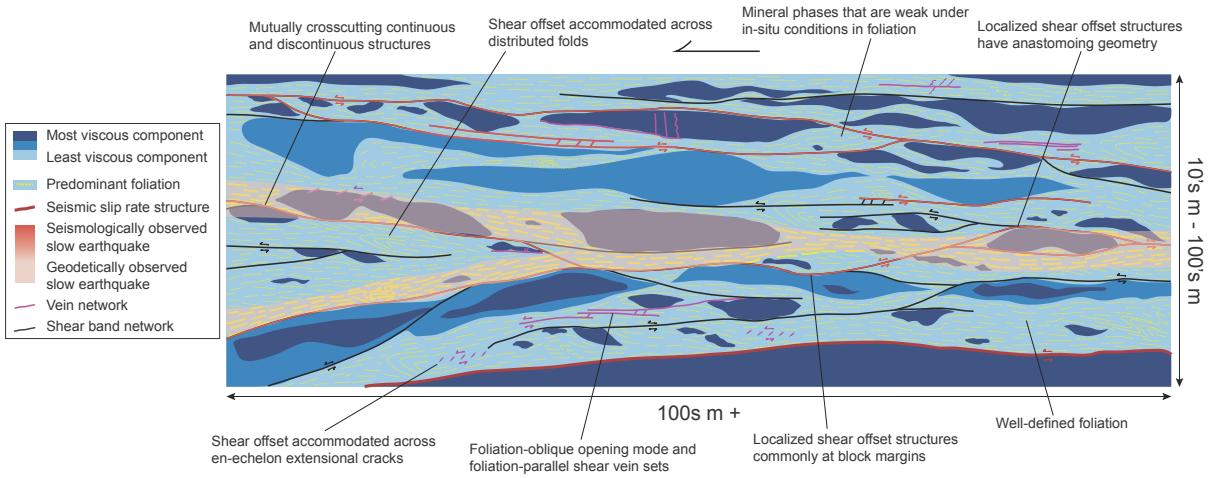

Figure 6. Schematic diagram showing the general characteristics of a slow earthquake structure. Potential shear zone that might accommodate a geodetically observed earthquake shown with shaded orange region. Networks of localized shear bands that could host seismologically observed earthquakes are shown in black. Examples of possible individual LFE rupture geometries are shown in red. Structures that might host large seismic slip shown in crimson. Magenta lines indicate opening-mode veins and portions of localized shear structures that may be mineralized and preserved as veins. The high strain zone contains units of different viscosity (blue shades), which are boudinaged, folded, and disrupted into blocks. The least viscous component indicated may be composed of a distinct lithology or a combination of lithologies (i.e. a mixture of matrix and small blocks as shown in FIG. 2E).

TABLE 1. ***Geology from Geophysics***

Seismological, geodetic, and geophysical data are the primary sources of information describing the sources of slow earthquakes[45-47]. The table below summarizes some predictions regarding the geological characteristics of the deformation structures that form or are reactivated during slip at slow to intermediate velocities based on these primary sources. Expected geological characteristics in italics are speculative. We note that the observations and interpretations outlined in the table should not be considered limiting, especially as new geophysical observations will cause the corresponding interpretations to evolve.

Box 1 Table. Geophysical constrain some of the environmental conditions at slow earthquake sources,

Geophysical observation	**Interpretation**	**Expected Geological/Structural characteristic**
Waveforms of seismologically observed slow earthquakes		
Radiated seismic energy[2,74]	Dynamic fracture, slip at seismic slip rates (>1mm/s)[173,174]	Fracture, frictional sliding potentially including evidence for dynamic weakening mechanisms
LFE waveforms[48,50]	Modeling suggests a double-couple mechanism, which implies dominantly shear	Apparent shear offset on a single structure or accommodated

	failure at source consistent with local active faults[48,50]	across a network of subparallel structures
Depletion in high-frequency radiated energy (low corner frequency)[67,175,176]	Low rupture velocity (potentially emphasized by a nearfield path with high preferential attenuation at high frequencies)	*Unusually smooth fault surfaces? Dilation during shear lowering pore pressure and increasing fault strength (dilatant strengthening)?*
Low stress drops for LFEs[67]	Low displacement/length ratio for slip events, slip under low friction and/or high fluid pressure[67]	Slip/length ratios of 10^{-6} – 10^{-5} for individual slip increments
Hypocentral locations distributed across zones 100s to 1000s m thick (note, however, thickness of the zone of hypocenter locations in most cases is similar to location uncertainty)[51,177]	Broad shear zone containing shear failure or multiple closely spaced structures is allowed, but not determined by the geophysical (seismic) data	Fault rock or other high strain feature of the order of 100s m thick containing evidence for numerous structures hosting intermediate slip rates

Tremor migration patterns (propagation rates of <1 to 100 km/hr)[82,178]	Large regions of host structures are critically stressed[82]	Prevalence of critically stressed structures with respect to ambient stress field
Tremor bursts	Multiple LFEs in a short period of time, potentially with each LFE limited in extent by some regulating mechanism[3]	Incremental offsets across a single structure and/or multiple, closely spaced structures that slip in same phase of deformation
Tremor recurrence interval decreases downdip[24,179,180]	Decrease in fault strength and/or tendency toward more stable or continuous slip downdip[24,62]. Possible silica redistribution and permeability decrease in downdip direction[179].	Temperature-sensitive deformation mechanisms. Veins, silicified fault rocks systematically changing in abundance with P-T conditions
Estimated magnitude range (≤M2?)[65,181]	Dimensions of up to hundreds of meters[175]	Continuous structure or network of structures corresponding to the dimension of the rupture
Other geophysical observables		

Spatial and temporal correspondence of tremor and SSE or afterslip[71,182,183]	Fracture and slip associated with strain rate perturbations	Structures representing low to intermediate strain rate coeval with fracture, mutually overprinting for repeated events, cyclical deformation
Modulation of low frequency events by tidal or teleseismic stress changes[78,184,185]	Small stress perturbations required to transition to fracture	Critically stressed structures with respect to ambient stress field possible, fluid-rich and high pore pressure environment recorded by veins, syn-kinematic mineralization
High Vp/Vs, high attenuation in slow earthquake source region[73-76]	High pore fluid pressure	Rock alteration/metamorphism, vein formation. Faults sealed by phyllosilicates(?) or mineralized by, e.g., quartz
Anisotropy of seismic velocity leading to shear wave splitting[186,187]	Aligned grains, mechanical anisotropy	Grain shape preferred orientation (and/or crystallographic preferred orientation), aligned meso-scale structures

References for figures

	Thermal Model	Seismological observations
1	Japan Trench/Kurile[188]	Tremor, LFEs, VLFEs[189-191]
2	Nankai, Kii (updip)[172]	Tremor, VLFEs[192-194]
3	Nankai, Kii (downdip)[172]	Tremor, LFEs, VLFEs[5,74,195]
4	Nankai, Shikoku (downdip)[172]	Tremor, LFEs, VLFEs[5,30,195]
5	Costa Rica[196]	Tremor, LFEs[51,53,197]
6	Central Ryukyu[198]	LFEs, VLFEs[199-201]
7	Hikurangi[202]	Tremor[14,203]
8	Mexico[204]	Tremor, LFEs[66,205,206]
9	Cascadia[172]	Tremor, LFEs, VLFEs[48,207,208]
10	Alpine Fault, New Zealand[209]	Tremor, LFEs[56,57,210]
11	Lishan Fault, Taiwan[211]	Tremor, LFEs[212-214]
12	San Jacinto Fault, USA[215]	Tremor[20,22,216]
13	San Andreas Fault, USA[217]	Tremor, LFEs[52,61,69]
14	Nankai Prism[218]	Tremor, VLFEs[11,15,16]

1450